Exocyclic Deoxyadenosine Adducts of 1,2,3,4-Diepoxybutane: Synthesis, Structural Elucidation, and Mechanistic Studies

Uthpala Seneviratne,[†,‡] Sergey Antsypovich,[†,§] Melissa Goggin,[†] Danae Quirk Dorr,[†,||] Rebecca Guza,[†] Adam Moser,[‡] Carrie Thompson,[†] Darrin M. York,[‡] and Natalia Tretyakova*[,†]

Department of Medicinal Chemistry and Masonic Cancer Center, and Department of Chemistry, University of Minnesota, Minneapolis, Minnesota 55455

Received September 1, 2009

1,2,3,4-Diepoxybutane (DEB) is considered the ultimate carcinogenic metabolite of 1,3-butadiene, an important industrial chemical and environmental pollutant present in urban air. Although it preferentially modifies guanine within DNA, DEB induces a large number of A → T transversions, suggesting that it forms strongly mispairing lesions at adenine nucleobases. We now report the discovery of three potentially mispairing exocyclic adenine lesions of DEB: N^6,N^6-(2,3-dihydroxybutan-1,4-diyl)-2′-deoxyadenosine (compound **2**), 1,N^6-(2-hydroxy-3-hydroxymethylpropan-1,3-diyl)-2′-deoxyadenosine (compound **3**), and 1,N^6-(1-hydroxymethyl-2-hydroxypropan-1,3-diyl)-2′-deoxyadenosine (compound **4**). The structures and stereochemistry of the novel DEB-dA adducts were determined by a combination of UV and NMR spectroscopy, tandem mass spectrometry, and independent synthesis. We found that synthetic N^6-(2-hydroxy-3,4-epoxybut-1-yl)-2′-deoxyadenosine (compound **1**) representing the product of N^6-adenine alkylation by DEB spontaneously cyclizes to form **3** under aqueous conditions or **2** under anhydrous conditions in the presence of an organic base. Compound **3** can be interconverted with **4** by a reversible unimolecular pericyclic reaction favoring **4** as a more thermodynamically stable product. Both **3** and **4** are present in double stranded DNA treated with DEB in vitro and in liver DNA of laboratory mice exposed to 1,3-butadiene by inhalation. We propose that in DNA under physiological conditions, DEB alkylates the N-1 position of adenine in DNA to form *N*1-(2-hydroxy-3,4-epoxybut-1-yl)-adenine adducts, which undergo an S_N2-type intramolecular nucleophilic substitution and rearrangement to give **3** (minor) and **4** (major). Formation of exocyclic DEB−adenine lesions following exposure to 1,3-butadiene provides a possible mechanism of mutagenesis at the A:T base pairs.

Introduction

Exocyclic nucleobase adducts are among the most important types of DNA damage because of their ability to exert significant biological effects (*1*−*3*). These lesions are characterized by considerable changes of the molecular size/shape and hydrogen bonding characteristics of the parent nucleobase, leading to mispairing during DNA synthesis (*4*−*9*). For example, 1,N^6-etheno-deoxyadenosine adducts induced by vinyl chloride preferentially adopt the *syn* conformation about the glycosidic bond, forming a Hoogsteen base pair with guanine or cytosine instead of the normal adenine partner, thymine (*4, 10*).

One prominent *bis*-electrophile capable of inducing exocyclic nucleobase lesions is 1,2,3,4-diepoxybutane (DEB[1]), the proposed ultimate carcinogenic metabolite of 1,3-butadiene (BD) (*11*). 1,3-Butadiene is a known animal and human carcinogen found in automobile exhaust and in cigarette smoke (*12, 13*). All three possible stereoisomers of DEB, *S*,*S*, *R*,*R*, and *meso*, are generated metabolically (*14*). Although DEB is a relatively minor metabolite of BD (laboratory mice exposed to 62.5 ppm BD for 10 days contain ∼247 pmol DEB/g blood (*15*)), experimental evidence suggests that it is responsible for many of the adverse effects of BD. DEB is 50−100-fold more genotoxic and mutagenic in human cells than its monoepoxide analogues, 3,4-epoxy-1-butene (EB) and 3,4-epoxy-1,2-butanediol (EBD) (*16, 17*). Efficient metabolism of BD to DEB in target tissues of laboratory mice is thought to cause the increased susceptibility of this species to BD carcinogenesis (*18*).

* Corresponding author. Masonic Cancer Center, University of Minnesota, MMC 806, 420 Delaware St. S.E., Minneapolis, MN 55455. Tel: (612) 626-3432. Fax: (612) 626-5135. E-mail: trety001@umn.edu.

† Department of Medicinal Chemistry and Masonic Cancer Center.

‡ Department of Chemistry.

§ Current address: Department of Chemistry, Moscow State University, Moscow, Russia.

|| Current address: Department of Chemistry and Geology, Minnesota State University, Mankato, MN.

[1] Abbreviations: **1**, N^6-(2-hydroxy-3,4-epoxybut-1-yl)-2′-deoxyadenosine (N^6-HEB-dA); **2**, N^6,N^6-(2,3-dihydroxybutan-1,4-diyl)-2′-deoxyadenosine (N^6,N^6-DHB-dA); **3**, 1,N^6-(2-hydroxy-3-hydroxymethylpropan-1,3-diyl)-2′-deoxyadenosine (1,N^6-γ HMHP-dA); **4**, 1,N^6-(1-hydroxymethyl-2-hydroxypropan-1,3-diyl)-2′-deoxyadenosine (1,N^6-α HMHP-dA); BCNU, 1,3-*bis*(2-chloroethyl)-1-nitroso-urea; *bis*-N7G-BD, 4-*bis*-(guan-7-yl)-2,3-butanediol; BD, 1,3-butadiene; $BzNH_2$, benzylamine; dA, 2′-deoxyadenosine; DEB, 1,2,3,4-diepoxybutane; DIPEA, *N*,*N*-diisopropylethyl amine; DFT, density functional theory; DMSO, dimethylsulfoxide; dR, 2′-deoxyribose; EtOH, Ethanol; Fmoc, 9-fluorenylmethoxycarbonyl; gCOSY, $^1H-^1H$ gradient correlation spectroscopy; gHMBC, gradient heteronuclear multiple bond correlation; gHMQC, gradient heteronuclear multiple quantum correlation; HEB, 2-hydroxy-3,4-epoxybut-1-yl; HOMO, highest occupied molecular orbital; HPLC-ESI-MS, high pressure liquid chromatography−electrospray ionization mass spectrometry; HSQC, heteronuclear single quantum correlation; *m*CPBA, *m*-chloroperoxybenzoic acid; MeOH, methanol; N7G-N1A-BD, 1-(guan-7-yl)-4-(aden-1-yl)-2,3-butanediol; NOESY, nuclear Overhauser effect spectroscopy; PyBOP, benzotriazol-1-yloxy-tripyrrolidinophosphonium hexafluorophosphate; SPE, solid phase extraction; THF, tetrahydrofuran; TMS-CN, trimethylsilyl cyanide; TOCSY, total correlation spectroscopy.

10.1021/tx900312e CCC: $40.75
Published on Web 11/02/2009

Chart 1.

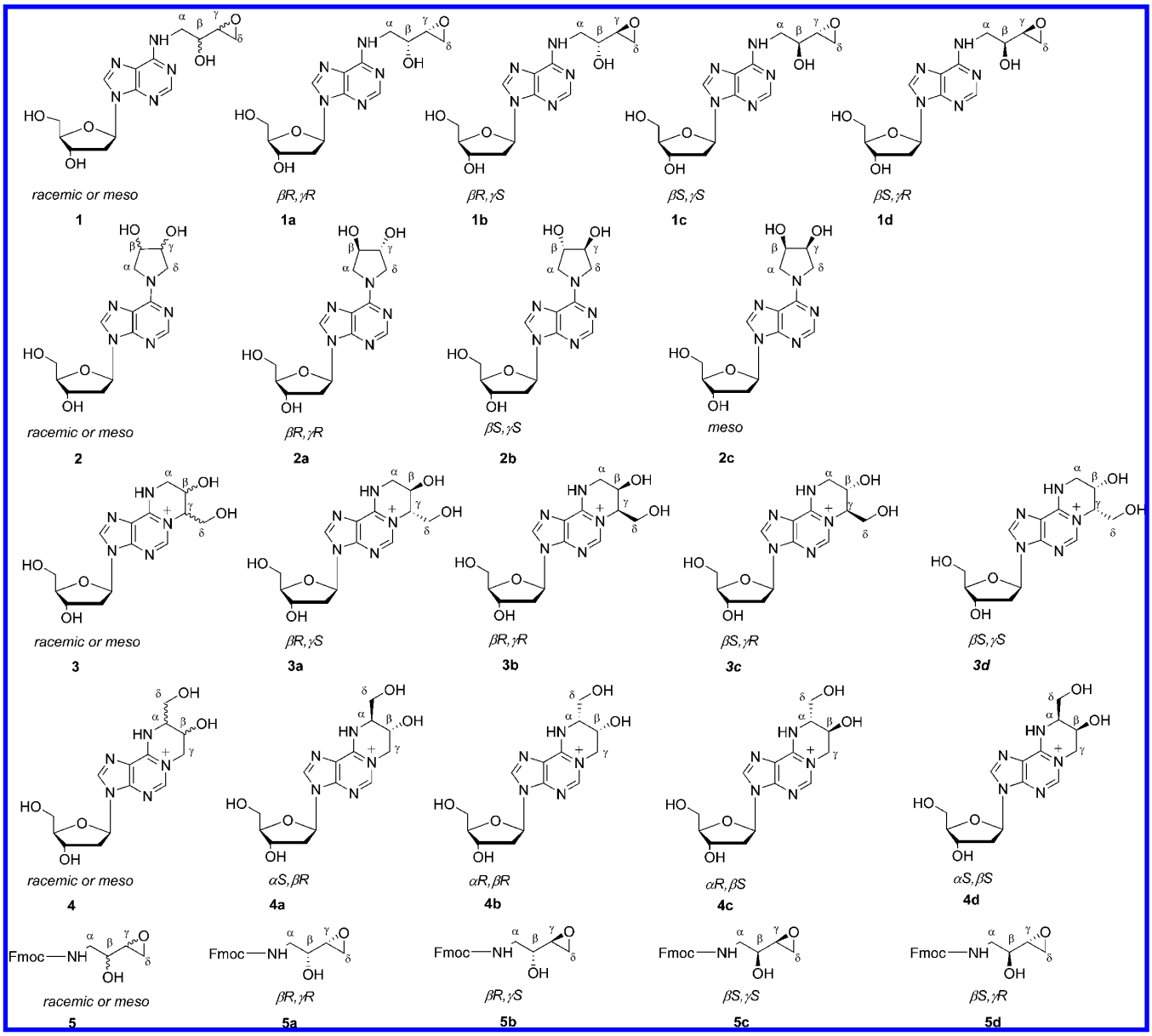

The adverse biological effects of DEB have been attributed to its ability to cross-link cellular biomolecules. Initial alkylation of adenine and guanine bases in DNA by DEB produces 2-hydroxy-3,4-epoxybut-1-yl (HEB) lesions, which contain an inherently reactive oxirane group and can alkylate neighboring nucleobases within the DNA duplex to form DNA−DNA cross-links, namely, 1,4-bis-(guan-7-yl)-2,3-butanediol (*bis*-N7G-BD) and 1-(guan-7-yl)-4-(aden-1-yl)-2,3-butanediol (N7G-N1A-BD) (*19, 20*). The *S*,*S* isomer of DEB produces the highest number of interstrand DNA−DNA cross-links (*21*) and is the most cytotoxic (*22, 23*) and mutagenic (*24*). Alternatively, the 3,4-epoxy group of the HEB adducts can be subject to nucleophilic attack by another site within the same DNA nucleobase, giving rise to fused ring structures (*25*−*27*).

The documented ability of DEB to induce large numbers of A → T transversion mutations (*28, 29*) has led us to hypothesize that it forms strongly mispairing exocyclic lesions at adenine nucleobases within DNA. This hypothesis was supported by our previous work with synthetic DNA oligonucleotides containing site specific N^6-(2-hydroxy-3,4-epoxybut-1-yl)deoxyadenosine adducts (N^6-HEB-dA, **1** in Chart 1) (*30*). If left in an aqueous solution at room temperature (pH 7.2), **1** underwent spontaneous cyclization to form previously unidentified DEB-dA lesions (see Supporting Information Figure S-1). Another isomer of the exocyclic DEB-dA species was formed as a side product during the synthesis of compound **1** (by reacting 6-chloropurine-2′-deoxyriboside with 1-amino-2-hydroxy-3,4-epoxybutane under basic, anhydrous conditions) (*30*). In the present work, we employed a combination of UV and NMR spectroscopy, tandem mass spectrometry, independent synthesis, DFT calculations, and kinetic analyses to identify the chemical structures of these novel DEB−DNA lesions and to establish the mechanism of their formation.

Materials and Methods

2′-Deoxyinosine was obtained from Berry & Associates, Inc. (Dexter, MI). $^{15}N_5$-dA was purchased from Spectra Stable Isotopes, Div. of Spectra Gases Inc. (Columbia, MD). *d*,*l*-DEB was obtained from the NCI Chemical Carcinogen Repository, and the individual stereoisomers of DEB were prepared as described previously (*21*). All other chemicals and enzymes were purchased from Sigma-Aldrich Chemical Co. (Milwaukee, WI).

Instrumentation. NMR spectra were acquired with a Varian Inova 600 MHz, 800 MHz spectrometer (Varian Inc., Palo Alto,

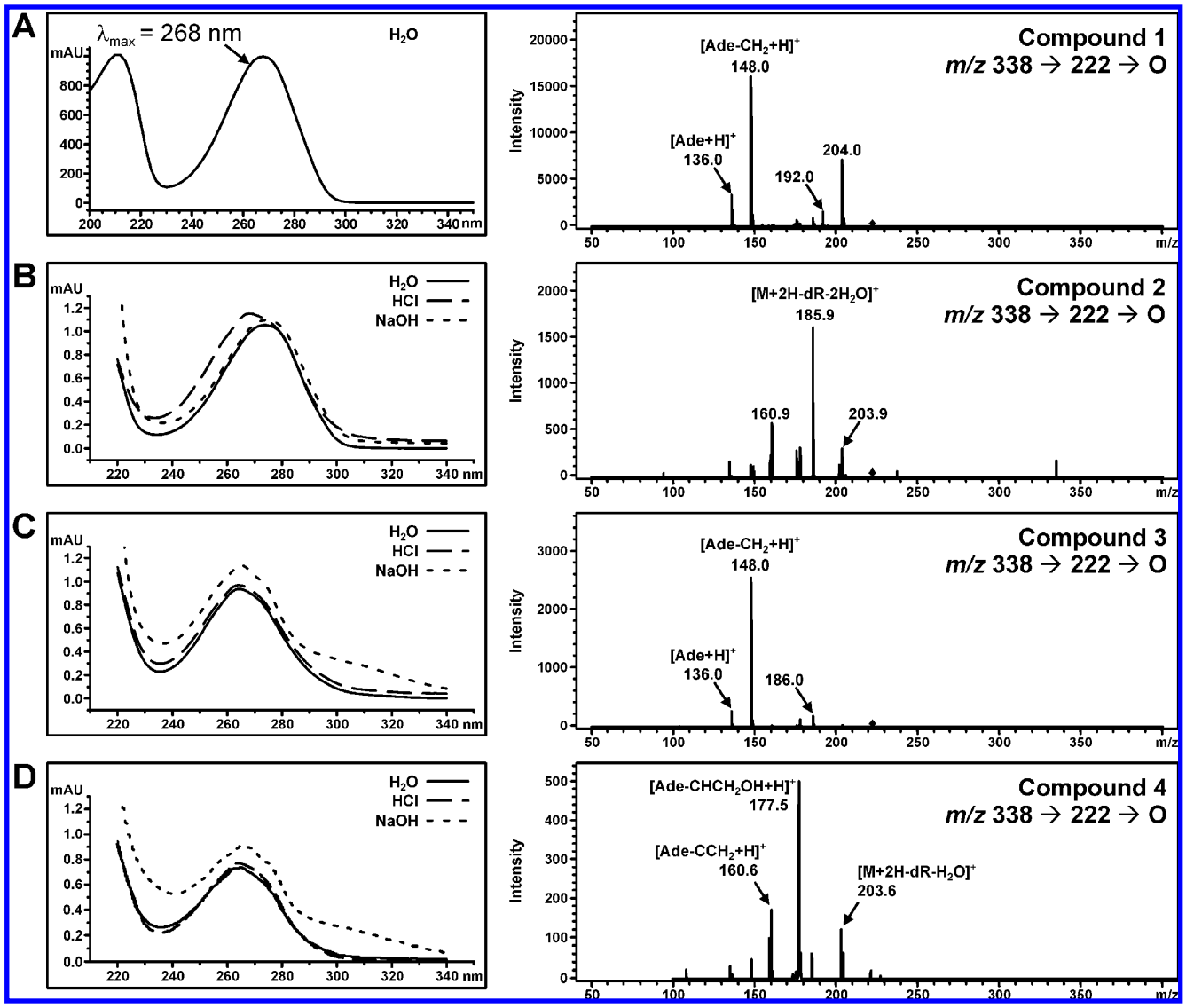

Figure 1. UV (left panel) and MS^3 spectra (right panel) of synthetic compounds **1** (A), **2** (B), **3** (C), and **4** (D).

CA) and a Bruker Advance 700 MHz instrument (Bruker BioSpin, Billerica, MA) using DMSO-d_6 as the solvent. UV spectrophotometry was performed on a Beckman DU-7400 instrument (Beckman, Fullerton, CA). Optical rotation mesurements were performed with a Rudolph Autopol III automatic polarimeter at 589 nm (Rudolph Research, Flanders, NJ), and HRMS data were obtained using a Bruker Bio-TOF II instrument.

HPLC-UV Analyses. HPLC was carried out with an Agilent Technologies model 1100 HPLC system equipped with a photodiode array UV detector (Wilmington, DE). Unless specified otherwise, UV absorbance was monitored at 254 nm. HPLC columns and solvent elution systems were as follows.

System 1. A semipreparative Zorbax Eclipse XDB-C18 (25 cm × 9.4 mm, 5 μm) column was eluted with a linear gradient of acetonitrile (B) in water (A) at a flow rate of 3 mL/min. Solvent composition was changed from 5% to 10.3% B in 35 min, then further to 90% B in 2 min. This system was used for the isolation of exocyclic DEB-dA adducts (compounds **1** and **2**) and the corresponding free bases. To separate **2a** from **2b**, the same column with an isocratic elution of 3% acetonitrile in water was used.

System 2. A preparative silica Whatman Particil 10 (50 cm × 9.4 mm, 10 μm) column was eluted isocratically with 0.5% methanol in chloroform at a flow rate of 5 mL/min. This system was used to separate the diastereomers of *N*-Fmoc-1-amino-2-hydroxy-3,4-epoxybutanes (compounds **5a**, **5b**, **5c**, and **5d**).

System 3. A 100 mm × 3 mm Thermo Hypersil Hypercarb column (10 cm × 3 mm, 5 μm particle size, Thermo Fisher Scientific, Inc. Waltham, MA) was eluted with a linear gradient of acetonitrile (B) in 0.05% acetic acid (A). Solvent composition was changed from 0 to 20% B in 30 min. The column was eluted at a flow rate of 0.5 mL/min. This system was used for the separation of **3** and **4** and the corresponding free bases.

Synthesis of *N*-Fmoc-1-Amino-2-hydroxy-3,4-epoxybutane, 5a−5d (Scheme 4). Racemic 1-aminobut-3-ene-2-ol was prepared from acrolein as described previously (*31*) and separated by diastereomeric resolution following derivatization with sodium [(1*R*)-(*endo*, *anti*)]-(+)-3-bromocamphor-8-sulfonic acid ammonium salt (*32, 33*), followed by Fmoc protection and epoxidation in the presence of *m*CPBA (*30*). Individual stereoisomers of the amino epoxide were isolated by preparative HPLC on a silica column (HPLC system 2). **5a**, $[\alpha]^{25}_D$ +4.0 (in $CHCl_3$), ee = 100%; **5b**, $[\alpha]^{25}_D$ −5.7 (in $CHCl_3$), ee = 100%; **5c**, $[\alpha]^{25}_D$ −3.4 (in $CHCl_3$), ee = 92.5% and **5d**, $[\alpha]^{25}_D$ +3.9 (in $CHCl_3$), ee = 84.2%.

Synthesis of N^6,N^6-DHB-dA (Scheme 1 and Chart 1). *S*,*S*-, *R*,*R*-, and *meso*-N^6,N^6-DHB-dA (compounds **2a**−**c** in Chart 1) were obtained by coupling commercial 6-chloropurine-2′-deoxyriboside with *S*,*S*-, *R*,*R*-, or *meso*-1-amino-2-hydroxy-3,4-epoxybutane, respectively (Scheme 1) (*30*). 6-Chloropurine-2′-deoxyriboside (1.45 mg, 5.36 μmol) was dissolved in DIPEA (18.7 μL), and *N*-Fmoc-1-amino-2-hydroxy-3,4-epoxybutane (6.95 mg, 21.4 μmol) dissolved in DMSO (200 μL) was added. The reaction mixture was incubated at 37 °C for 2 days under Ar atmosphere. The reaction products were diluted with water, filtered, and separated using HPLC system 1. Under these conditions, *R*,*R*- and *S*,*S*-N^6,N^6-DHB-

dA (compounds **2a** and **2b**) eluted at 15.4 min, while *meso*-N^6,N^6-DHB-dA (compound **2c**) was observed as a peak at 16.7 min (2.95 mg, 8.73 μmol, 40.8%). Compounds **2a** and **2b** were resolved with a different HPLC system (3% ACN in water): **2a**, t_R, 55.1 min (1.59 mg, 22.0% yield),) and **2b**, t_R, 56.6 min (1.74 mg, 24.0% yield). UV (water): λ_{max} = 274 nm (Figure 1, left), ESI$^+$-MS *m*/*z* 338.3 [M + H]$^+$; MS/MS *m*/*z* 338.3 → 222.2 [M + 2H-dR]$^+$; MS^3 *m*/*z* 338.3 → *m*/*z* 222.2 → *m*/*z* 136.0 [Ade + H]$^+$, 147.6 [Ade-CH_2 + H]$^+$, 185.6 [M + 2H-dR-2H_2O]$^+$, 204.0 [M + 2H-dR-H_2O]$^+$ (Figure 1, right panel).

^{1}H NMR (DMSO-d_6), compound **2a** (*S*,*S* N^6,N^6-DHB-dA): 8.32 (s, 1H, *H*-8); 8.18 (s, 1H, *H*-2); 6.35 (t, 1H, *H*-1′, J_{vic} = 6.96 Hz); 5.30 (d, 1H, CHO*H*-3′, J_{vic} = 3.66 Hz); 5.22 (t, 1H, CHO*H*-5′, J_{vic} = 5.50 Hz); 5.19 (bs, 1H, CHOH^{β}); 5.17 (bs, 1H, CHOH^{γ}); 4.40 (bs, 1H, *H*-3′); 4.17 (d, 1H, H^{α}, J_{gem} = 12.21 Hz); 4.09 (m, 1H, H^{β}); 4.01 (m, 2H, H^{α}, H^{γ}); 3.87 (d, 1H, *H*-4′, J_{vic} = 2.69 Hz); 3.68 (m, 1H, H^{δ}); 3.62 (m, 2H, H^{δ}, *H*-5′); 3.51 (m, 1H, *H*-5′); 2.69 (q, 1H, *H*-2′); 2.26 (dq, 1H, *H*-2′, J_{gem} = 13.18 Hz).

^{1}H NMR (DMSO-d_6), compound **2b** (*R*,*R* N^6,N^6-DHB-dA): 8.32 (s, 1H, *H*-8); 8.18 (s, 1H, *H*-2); 6.35 (t, 1H, *H*-1′, J_{vic} = 6.84 Hz); 5.22 (bs, 4H, O*H*-groups); 4.40 (q, 1H, *H*-3′, *J* = 2.85 Hz); 4.17 (bd, 1H, H^{α}, *J* = 12.6 Hz); 4.10 (bs, 1H, H^{β}); 4.02 (bs, 1H, H^{α}); 4.00 (bs, 1H, H^{γ}); 3.87 (q, 1H, *H*-4′, *J* = 4.2 Hz); 3.69 (bd, 1H, H^{δ}); 3.63 (m, 1H, H^{δ}); 3.61 (m, 1H, *H*-5′); 3.51 (dd, 1H, *H*-5′, J_1 = 11.70 Hz, J_2 = 4.50 Hz); 2.68 (m, 1H, *H*-2′); 2.25 (dq, 1H, *H*-2′, J_1 = 13.20 Hz, J_2 = 3.20 Hz).

^{1}H NMR (DMSO-d_6), compound **2c** (*S*,*R* and *R*,*S* N^6,N^6-DHB-dA): 8.33 (s, 1H, *H*-8); 8.19 (s, 1H, *H*-2); 6.36 (t, 1H, *H*-1′, J_{vic} = 6.9 Hz); 5.31 (d, 1H, CHO*H*-3′, J_{vic} = 4.2 Hz); 5.21 (t, 1H, CHO*H*-5′, J_{vic} = 5.7 Hz); 5.03 (d, 1H, CHOH^{β}, J_{vic} = 3.7 Hz); 4.96 (bs, 1H, CHOH^{γ}); 4.40 (m, 1H, *H*-3′, J_1 = 5.7 Hz; J_2 = 2.9 Hz); 4.21 (d, 1H, H^{α}, J_{gem} = 12.0 Hz); 4.17 (bs, 1H, H^{β}); 4.13 (bs, 1H, H^{γ}); 3.91 (d, 1H, H^{α}, J_{gem} = 10.2 Hz); 3.88 (q, 1H, *H*-4′, J_{vic} = 4.2 Hz); 3.72 (d, 1H, H^{δ} J_{gem} = 12.0 Hz); 3.61 (m, 2H, *H*-5′, H^{δ}, J_{gem} = 11.71 Hz; J_{vic}= 4.4 Hz); 2.70 (m, 1H, *H*-2′, J_{gem} = 13.2 Hz; J_{vic} = 6.3 Hz); 2.26 (m, 1H, *H*-2′, J_{gem} = 13.2 Hz; J_{vic} = 6.6 Hz).

Computational Methods. Density-functional electronic structure calculations were performed according to the protocol used in the QCRNA database (*34*). The calculations included geometry optimization, vibrational frequency analysis, and solvation energy corrections. Kohn−Sham density-functional calculations were performed using the hybrid exchange functional of Becke (*35*) and the Lee, Yang, and Parr correlation functional (*36*) (B3LYP) as implemented in the Gaussian 03 suite of programs (see http://www.gaussian.com/citation_g03.htm). Relaxed potential energy surface scans around the C−N torsion angle were performed at the B3LYP/6-31+G(d,p) level with the torsion constraint set in 15° intervals, with additional unconstrained (fully optimized) points at the minima.

Molecular orbitals for the axial, equatorial, and pucker transition state structures of **2a-base** were calculated. All structures showed at least 7 orbitals with significant density above and below the C−N σ bond. Supporting Information Figures S-12A and S-12B show a top view and side view of two molecular orbitals (HOMO-2 and HOMO-20) of compound **2a-base** in an equatorial-like conformation.

Independent Synthesis of Compounds 2a, 2b, and 2c (Scheme 2). 3*R*,4*R*-Pyrrolidine-2,3-diol (125 mg, synthesized as described previously) (*37, 38*) was coupled with 2′-deoxyinosine (250 mg) in the presence of DMSO (5 mL), DIPEA (210 μL), and PyBOP (656 mg) (55 °C for 3 days). The reaction mixture was resolved by flash chromatography (CH_2Cl_2/MeOH solvent gradient using a silica column) and reversed phase HPLC (system 1) to give optically pure (*R*,*R*)-N^6,N^6-DHB dA, $[\alpha]^{25}_D$ +43.0 (in MeOH) (**2a**) in 72% yield. The same synthetic route starting with L-tartaric acid and *meso*-tartaric acid was followed to obtain the optically pure (*S*,*S*)-N^6,N^6-DHB dA, $[\alpha]^{25}_D$ −42.8 (in MeOH) (**2b**) and *meso*-N^6,N^6-DHB dA, $[\alpha]^{25}_D$ −19.4 (in MeOH) (**2c**), respectively.

Synthesis of *R*,*R* (1a)-, *R*,*S* (1b)-, *S*,*S* (1c)-, and *S*,*R* (1d)-N^6-HEB-dA. Compounds **5a**−**5d** (15 mg) (*37, 38*) were coupled with 2′-deoxyinosine (15 mg) in the presence of DMSO (1 mL), DIPEA (50 μL), and PyBOP (30 mg) (5 days at room temperature). The reaction mixtures were resolved by reversed phase HPLC (system 1) to give (*R*,*R*)-N^6-HEB dA, (**1a**), (*R*,*S*)-N^6-HEB dA, (**1b**), (*S*,*S*)-N^6-HEB dA, (**1c**), and (*S*,*R*)-N^6-HEB dA, (**1d**) separately in 95% yield.

Chart 2.

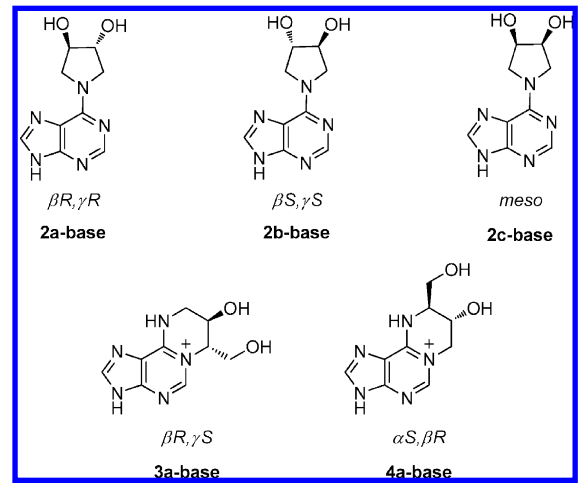

Synthesis of Compounds 3 and 4 in Chart 1. Racemic N^6-HEB-dA (compound **1** in Chart 1, 1.5 mg) (*30*) was dissolved in 250 μL of water and incubated for 15 h at room temperature. Spontaneous cyclization of N^6-HEB-dA produced **3** and **4**, which were isolated with HPLC system 3: **3**, t_R, 12.5 min and **4**, t_R, 16.8 min (**3**, 0.87 mg, 2.55 μmol, 57.3% yield and **4**, 0.57 mg, 1.67 μmol, 38.0% yield, ratio of **3**:**4**; 7:3). UV (pH 7) **3** and **4**, λ_{max} = 264 nm. Compound **3**: ESI$^+$-MS *m*/*z* 338.3 [M + H]$^+$, MS^2 *m*/*z* 338.3 → *m*/*z* 222.2 [M + 2H-dR]$^+$; MS^3 *m*/*z* 338.3 → *m*/*z* 222.2 → *m*/*z* 136.0 [Ade + H]$^+$, 148.0 [Ade-CH_2 + H]$^+$, 186.0 [M + 2H-dR-2H_2O]$^+$. Compound **4**: ESI$^+$-MS *m*/*z* 338.3 [M + H]$^+$, MS^2 *m*/*z* 338.3 → *m*/*z* 222.2 [M + 2H-dR]$^+$; MS^3 *m*/*z* 338.3 → *m*/*z* 222.2 → *m*/*z* 160.6 [Ade-CCH + H]$^+$, 177.5 [Ade-$(CH)_2$OH + H]$^+$, 203.6 [M + 2H-dR-H_2O]$^+$.

Synthesis of 3a−3d and 4a−4d. Compounds **1a**−**1d** were dissolved in 250 μL of water and incubated for 12 h at room temperature. The cyclization products were purified with HPLC system 3. Compounds **3a** and **4a** were obtained from the cyclization of **1a**; **3b**, and **4b** were obtained from the cyclization of **1b**; **3c**, and **4c** were obtained from the cyclization of **1c**; **3d**, and **4d** were obtained from the cyclization of **1d**. Compound **3a**, t_R, 12.5 min; **4a**, t_R, 16.8 min; **4b**, t_R, 19.6 min; and **3b**, t_R, 21.7 min; **3c**, t_R, 12.5 min; **4c**, t_R, 16.8 min; **4d**, t_R, 19.6 min; and **3d**, t_R, 21.7 min. The ^{1}H NMR, NOESY, gCOSY, gHSQC, and HMBC data for compounds **3a**, **3b**, **4a**, and **4b** are presented in Supporting Information Figures S-14−S-18.

$^{15}N_4$-Deoxyinosine. $^{15}N_5$-Deoxyadenosine (10 mg, 80 μmol) was incubated in the presence of adenosine deaminase (80 units) in 10 mM Tris-HCl, pH 7.4 (0.75 mL), at 37 °C for 24 h. HPLC analysis revealed a single peak corresponding to $^{15}N_5$-deoxyinosine. The mixture was filtered through a YM-30 Centricon filter to remove any protein and desalted using Waters C18 SPE cartridges (95% yield).

Synthesis of $^{15}N_4$-Labeled Compounds 3 and 4. To a solution of $^{15}N_4$-deoxyinosine (0.026 mmol, 6.5 mg) in DMSO (2.5 mL), PyBOP (0.026 mmol, 13.5 mg), DIPEA (0.11 mmol, 19 μL), and racemic compound **5** (0.022 mmol, 7 mg) was added (*39*). The mixture was stirred for 3 days at room temperature under argon to give $^{15}N_4$-N^6-HEB-dA. ESI$^+$-MS *m*/*z* 342.3 [M + H]$^+$, MS^2 *m*/*z* 342.3 → *m*/*z* 226.2 [M + 2H-dR]$^+$; MS^3 *m*/*z* 342.3 → *m*/*z* 226.2 → *m*/*z* 140.0 [$^{15}N_4$-HX + H]$^+$, 152.0 [$^{15}N_4$-HX-CH_2 + H]$^+$, 190.0 [M + 2H-dR-2H_2O]$^+$, 208.0 [M + 2H-dR-H_2O]$^+$. $^{15}N_4$-N^6-HEB-dA was quantitatively converted to $^{15}N_4$ -labeled compounds **3** and **4** by incubating in water overnight, followed by HPLC purification with HPLC system 3. Standard solutions of $^{15}N_4$-labeled **3** and **4** were prepared in water and quantified by UV spectrophotometry.

Scheme 1. Formation of 1, 2, 3, and 4 upon the Coupling of 6-chloropurine-2′-deoxyriboside with *N*-Fmoc-1-Amino-2-hydroxy-3,4-epoxybutane

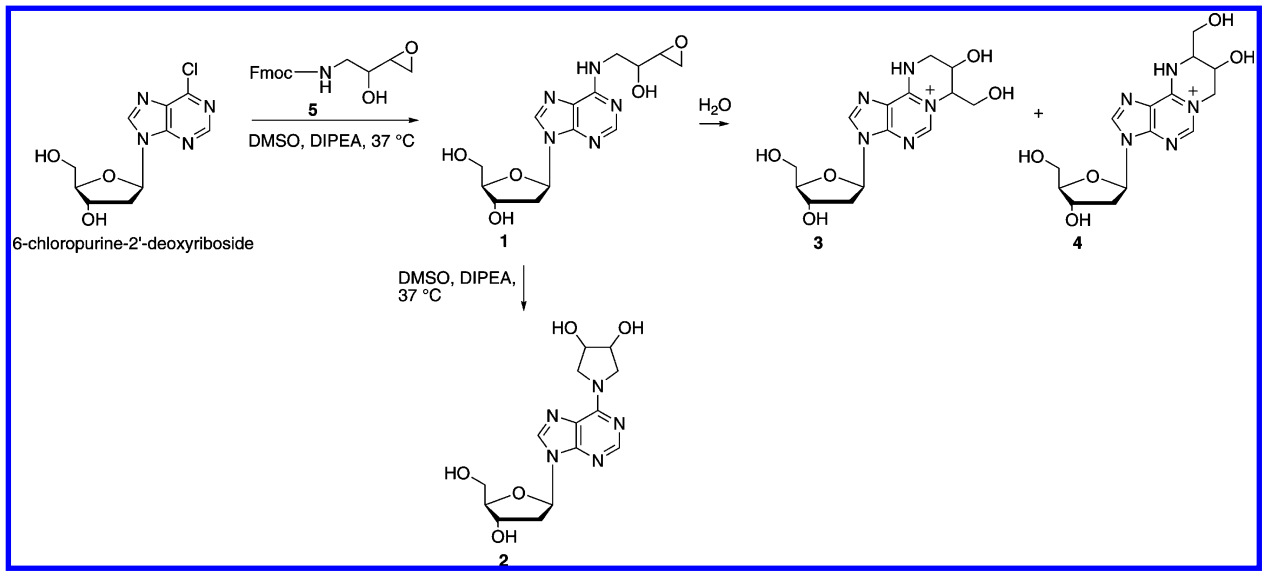

Forced Dimroth Rearrangement of 3a and 4a. Compounds **3a** and **4a** were separately dissolved in 200 μL of 0.25 M NaOH solution and kept at room temperature for 1 h, followed by neutralization with 1 M HCl. The reaction mixtures were then heated to 60 °C after the addition of 300 μL of 95% EtOH and kept for 4 more hours. About 8 μL was injected onto a capillary HPLC column for HPLC-ESI$^+$-MS/MS analysis.

Neutral Thermal Hydrolysis. Nucleoside adducts (0.1 mg each) were dissolved in 100 μL of water and heated for 1 h at 85 °C. The resulting reaction mixtures were separated with HPLC systems 1 and 3.

Synthesis of Nucleobase Adducts via Acid Hydrolysis of the Corresponding Nucleosides. Compounds **2a**, **2b**, **2c**, **3**, and **4** were dissolved in 0.1 M HCl (250 μL) and heated for 1 h at 85 °C. The resulting reaction mixtures were neutralized with 0.1 M NaOH and separated by HPLC (systems 1 and 3). Compound **2a-base** (Chart 2) was isolated as a peak at 7.7 min (0.62 mg, 2.78 μmol, 94.0% yield). Compound **2b-base** was isolated as a peak at 8.1 min (0.62 mg, 2.81 μmol, 95.0% yield). *S*,*R*; *R*,*S*-N^6,N^6-(2,3-dihydroxybutan-1,4-diyl)-adenine (**2c-base**, Chart 2) was isolated at 11.7 min (0.65 mg, 2.93 μmol, 99.0% yield). Compounds **2a-base**, **2b-base**, and **2c-base** had identical UV and mass spectra. UV (water): λ_{max} 274 nm; ESI$^+$-MS *m*/*z* 222.2 [M + H]$^+$, MS^2 of *m*/*z* 222.2: *m*/*z* 147.9 [Ade-CH_2 + H]$^+$, 160.6 [Ade-CH=CH_2]$^+$, 175.6 [Ade-CH_2−CH=CH_2+H]$^+$, 185.6 [M + 2H-dR-2H_2O]$^+$, 203.7 [M + 2H-dR-H_2O]$^+$.

Compound **3-base** was isolated at 8.4 min. λ_{max} 264 nm, ESI$^+$-MS: *m*/*z* 222.2 [M + H]$^+$, MS^2 of *m*/*z* 222.2: *m*/*z* 136.0 [Ade + H]$^+$, 148.0 [Ade-CH_2 + H]$^+$, 186.0 [M + 2H-dR-2H_2O]$^+$.

Compound **4-base** was isolated at 12.1 min. λ_{max} 264 nm, ESI$^+$-MS: *m*/*z* 222.2 [M + H]$^+$, MS^2 of *m*/*z* 222.2: *m*/*z* 160.6 [Ade-CCH + H]$^+$, 177.5 [Ade-$(CH)_2$OH + H]$^+$, 203.6 [M + 2H-dR-H_2O]$^+$.

The ^{1}H NMR, NOESY, gCOSY, TOCSY, gHMQC, and HSQC data for compounds **2a-base**, **2b-base**, and **2c-base** are presented in Supporting Information Figures S-8 and S-9.

Oxidation of 1,2-Diols with Sodium Periodate and Analysis of Oxidation Products by HPLC-ESI$^+$-MS/MS. Nucleobase adducts **2a-base**, **2b-base**, **2c-base**, **3-base**, and **4-base** (3 nmol aliquots) were dissolved in 15 mM aqueous sodium periodate (30 μL). Thymidine (0.1 ou_{260}) was added as an internal standard for quantitation. Aliquots (6 μL) were taken following incubation for 10 min, 1 h, 2 h, 4 h, and 23 h. The reaction was terminated by the addition of glycerol (1 μL), and the samples were frozen until HPLC-ESI$^+$-MS/MS analysis with an Agilent 1100 capillary HPLC-ion trap mass spectrometer system (Agilent Technologies, Inc.; Wilmington, DE). A 250 mm × 0.5 mm Synergi column, 4 μm particle size (Phenomenex, Torrance, CA) was eluted with a linear gradient of methanol (B) in 0.05% acetic acid (A). Solvent composition was changed from 0% to 1% B in 6 min, then further to 4% B in 11 min, and finally to 30% B in 2 min. The column was eluted at a flow rate of 12 μL/min. Oxidation products (dialdehyde derivatives and the corresponding hemiacetals) were detected by HPLC-ESI$^+$-MS: dialdehyde at *m*/*z* 220.2 [M + H]$^+$; MS^2 *m*/*z* 220.2 → *m*/*z* 202.0 [M+H -H_2O]$^+$, and hemiacetal at *m*/*z* 238.3 [M +H]$^+$, MS^2 *m*/*z* 238.3 → *m*/*z* 220.2 [M+H -H_2O]$^+$ (Supporting Information Figure S-2).

Table 1. pH Dependence of the UV Absorbance Spectra of Exocyclic DEB-dA Adducts

	UV_{max} (nm)		
compound	0.1 M HCl	water	0.1 M NaOH
2a	268	274	274
2b	268	274	274
2c	268	274	274
3a	264	264	265
3b	264	265	267
4a	264	265	266
4b	264	265	267

Kinetics of Cyclization of 1a and 1b in Aqueous Medium. Pure compounds **1a** or **1b** were dissolved in water and incubated at 37 °C. The reaction products were monitored by HPLC system 1 (**1a**, $t_{1/2}$ = 58 min; and **1b**, $t_{1/2}$ = 58 min, Supporting Information Figure S-19). In a separate experiment, **1a** was dissolved in water, and the formation of **3a** and **4a** was monitored by HPLC (system 3, Supporting Information Figure S-22).

Kinetics of the Conversion of 3a and 4b in Aqueous Medium. Purified **3a** and **4a** were incubated in water either at room temperature or at 37 °C, and the rearrangement products were detected by HPLC (Supporting Information Figure S-23).

HPLC-ESI-MS/MS Analysis of Exocyclic DEB-dA Adducts in DEB-Treated DNA. Calf thymus DNA (500 μg aliquots, in 500 μL of water) was treated with increasing amounts of *R*,*R*-, *S*,*S*-, and *meso*-DEB (0−1 mM) at 37 °C for 24 h. DNA was precipitated with cold ethanol and resuspended in 500 μL of water. Following spiking with $^{15}N_4$-labeled compounds **3** and **4** (500 fmol, internal standards for mass spectrometry), DNA was digested to deoxynucleosides in the presence of Nuclease P1 (10 U) and alkaline phosphatase (60 U, 37 °C for 1 h). Samples were filtered through YM-30 Centricon filters to remove proteins prior to solid phase extraction (SPE). Carbograph SPE cartridges (3 mL, Alltech) were prepared by washing with methanol (2 × 3 mL) and water (2 × 3 mL). Samples were loaded in water (1 mL), washed with water

Scheme 2. Stereospecific Synthesis of Compound 2a[a]

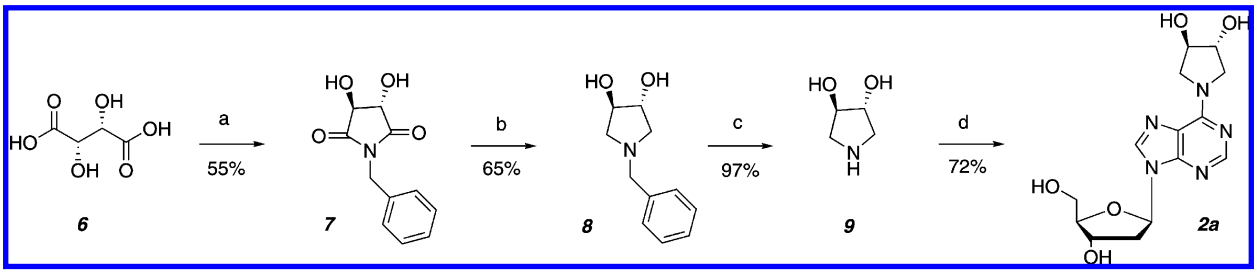

[a] (a) 1 equiv $BzNH_2$, *p*-xylene, reflux, 3 h; (b) LiAlH4, THF, 12 h; (c) H_2, 10% Pd−C, 55°C, 24 h; (d) 2′-deoxyinosine, DMSO, DIPEA, PyBOP, 55°C, 3 d.

and 10% methanol (3 mL each), and eluted with 30% methanol (3 mL). The 30% methanol elutions were concentrated under vacuum and redissolved in 25 μL of water. About 8 μL was injected onto a capillary HPLC column for HPLC-ESI$^+$-MS/MS analysis. Exocyclic DEB-dA adduct amounts were determined from the relative response ratios (mass spectrometry peak area of exocyclic DEB-dA adduct to mass spectrometry peak area of isotopically labeled internal standard).

HPLC-ESI-MS/MS Analysis of Exocyclic DEB-dA Adducts in Tissues of B6C3F1 Mice Exposed to BD by Inhalation. B6C3F1 mice were exposed to 625 ppm butadiene or air (controls) for 2 weeks, and liver DNA was isolated using NuceoBond AXG500 anion exchange cartridges (Macherey-Nagel) (*40*). DNA purity and amounts were determined by UV spectrophotometry. The A_{260}/A_{280} ratios were 1.7−1.8, confirming minimal protein contamination. DNA (100 μg) was spiked with $^{15}N_4$-labeled compounds **3** and **4** (300 fmol each) and subjected to enzymatic digestion as described above for CT DNA. Samples were filtered through YM-10 Centricon microfilters, purified by SPE as described above for CT DNA, dried under vacuum, and dissolved in 25 μL of water. About 8 μL was injected onto a capillary HPLC column for HPLC-ESI-MS/MS analysis as described above for CT DNA.

Liquid Chromatography−Mass Spectrometry. The majority of HPLC-ESI-MS experiments were performed with an Agilent 1100 capillary HPLC-ion trap mass spectrometer (Agilent Technologies, Inc., Wilmington, DE). The instrument was operated in the ESI$^+$ mode. Target ion abundance value was set to 30,000, the maximum accumulation time was 300 ms, and 4 scans were taken per average. A typical fragmentation amplitude was 0.7 V, with a scan width of 1.2 *m/z*. Nitrogen was used as a nebulizing (15 psi) and drying gas (5 L/min, 200 °C). Electrospray ionization was achieved at a spray voltage of 3−3.5 kV.

For analyses of nucleoside reaction mixtures, samples were dissolved in a 1:1 mixture of acetonitrile and 0.1% acetic acid, and infused at a flow rate of 10−15 μL/min using a syringe pump. The mass spectrometer was operated in full scan mode over the range of *m/z* 50−350.

Enzymatic digests of DEB-treated DNA and liver DNA from control and butadiene-exposed mice were analyzed with an Agilent 1100 capillary HPLC system (Wilmington, DE) interfaced to a Thermo-Finnigan TSQ Quantum Ultra mass spectrometer (Thermo Fisher Scientific Corp., Waltham, MA). A Phenomenex Synergi (250 × 0.5 mm, 0.4 μm) column was eluted with a gradient of 10 mM ammonium formate, pH 4.2 (A), and methanol (B). The solvent composition was kept at 100% A for 5 min, changed to 6% B over 1 min, and finally increased linearly to 30% B over 10 min. Under these conditions, **3** and **4** coeluted at 14.5 min, while **2** eluted at 41.1 min. In order to separate **3** and **4**, a capillary Thermo Hypercarb column (150 × 0.5 mm, 5 μm, Thermo Fisher Scientific, Inc. Waltham, MA) was eluted with 0.05% acetic acid, pH 4.0 (A), and 100% acetonitrile (B) at the same gradient. The mass spectrometer was operated in the positive ion mode, with nitrogen used as a sheath gas (5 L/min). Electrospray ionization was achieved at a spray voltage of 4.0 kV and a capillary temperature of 270 °C. CID was achieved with Ar as a collision gas (1 mTorr) and a collision energy of 35 V. The mass spectrometer parameters were optimized for maximum response during the infusion of standard solutions. Both exocyclic DEB-dA lesions were quantified by isotope dilution with the corresponding $^{15}N_4$-labeled internal standards. Quantitative analyses were performed in the selected reaction monitoring (SRM) mode using HPLC-ESI$^+$-MS/MS peak areas corresponding to the neutral loss of deoxyribose from protonated molecules of the adducts (*m/z* 338.1 $[M + H]^+ \rightarrow$ 222.0 $[M + 2H\text{-}dR]^+$ and *m/z* 342.1 $[M + H]^+ \rightarrow$ 226.0 $[M + 2H\text{-}dR]^+$ for analytes and their internal standards, respectively).

Results

Synthesis and Initial Characterization of Exocyclic DEB-dA Adducts. Three isomers of exocyclic DEB-dA lesions were initially prepared. One of them (compound **2** in Scheme 1) was isolated as a side product during the synthesis of compound **1**, which was accomplished by coupling 6-chloropurine deoxyriboside with 1-amino-2-hydroxy-3,4-epoxybutane in the presence of an organic base (Scheme 1) (*30*). Two additional DEB-dA exocycles (compounds **3** and **4**) were obtained as major products of spontaneous cyclization of **1** in an aqueous solution (Scheme 1) (*30*). All three exocyclic DEB-dA adducts **2**, **3**, and **4** had the same molecular weight (337.2 Da) as determined by ESI$^+$ MS (*m/z* 338, $[M + H]^+$), and their molecular formula from Q-TOF MS analysis was consistent with the addition of one molecule of DEB to deoxyadenosine ($C_{14}H_{19}N_5O_5$, calculated, *m/z* 338.1459; observed, *m/z* 338.1446).

Unlike compound **1**, which has a half-life of ∼100 min under physiological conditions (*30*), compounds **2**, **3**, and **4** were relatively stable in an aqueous solution at pH 7.2 (with the exception of the slow interconversion of **3** and **4**; see below). Moreover, no structural changes were observed following heating for 1 h at 85 °C (not shown). Acid hydrolysis (0.1 N HCl, 30 min at 85 °C) of nucleosides **2**, **3**, and **4** cleaved the deoxyribose, while the alkylated nucleobases retained the DEB moiety, indicating that both alkylation events took place within the adenine portion of the molecule.

Three stereoisomers of **2** (**2a**, **2b**, and **2c**) were synthesized (Chart 1). Compounds **2a** and **2b** originated from *R*,*R* + *S*,*S*-1-amino-2-hydroxy-3,4-epoxybutane (**5a** + **5c**) and were resolved by reversed phase HPLC. Compound **2c** was prepared from *meso*-1-amino-2-hydroxy-3,4-epoxybutane (**5b** + **5d**). The absolute configurations of compounds **2a**, **2b**, and **2c** were subsequently determined by the independent synthesis described below. The individual diastereomers of compounds **3** and **4** could not be resolved by conventional HPLC because of their polar character, which led to poor retention of these nucleosides on reversed phase HPLC columns. As described in a later section, stereospecific synthesis was subsequently used to prepare individual stereoisomers of compounds **3** and **4**.

To identify the substitution sites within the adenine heterocycle, electronic spectra of compounds **2**, **3**, and **4** under

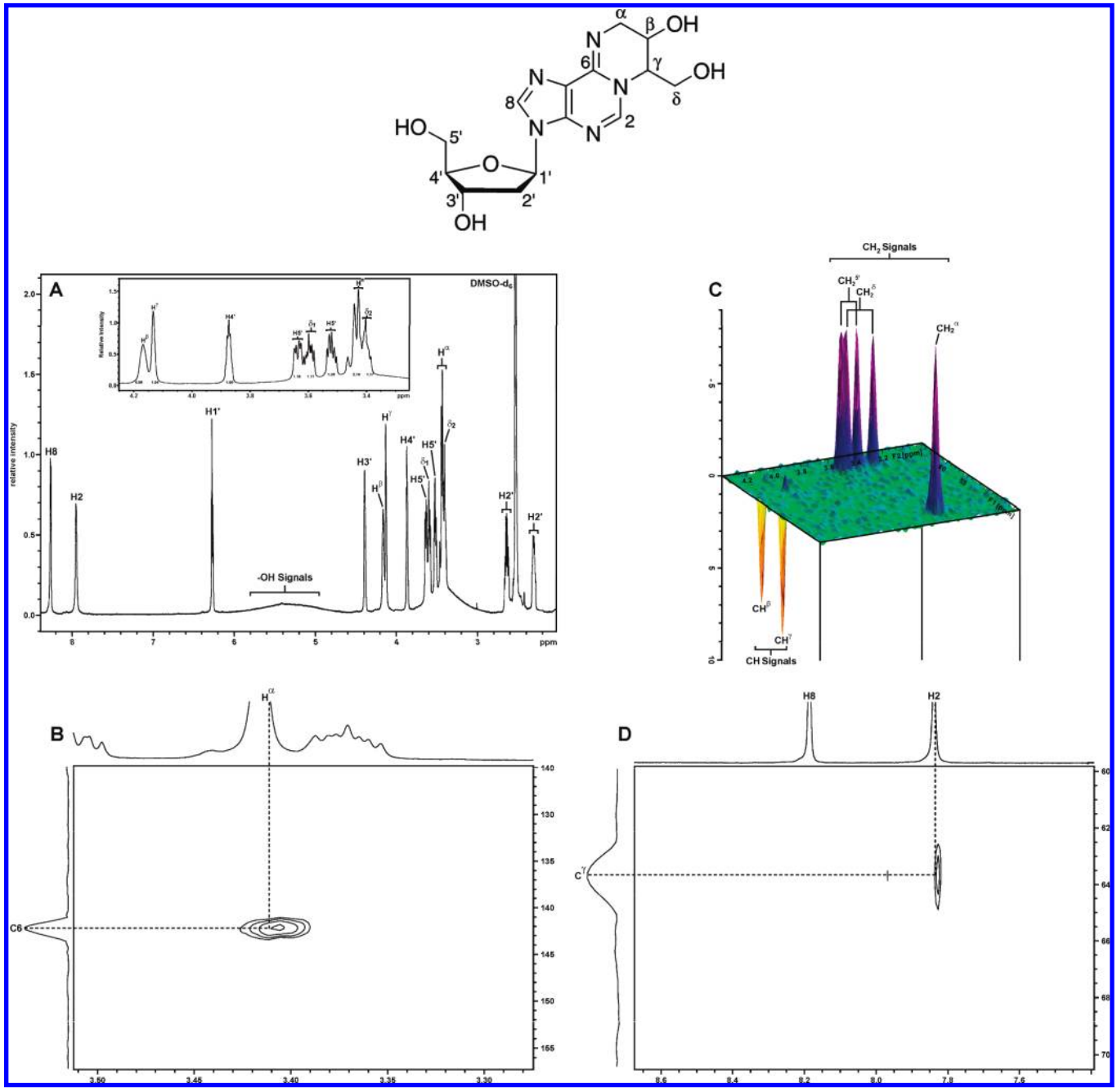

Figure 2. ^{1}H NMR (A), HMBC (B and D), and phase sensitive HSQC spectra (C) of compound **3** (racemic) (Bruker 700 MHz) (Inset in A: enlarged area of 3.2−4.3 ppm).

different pH conditions were examined. UV absorbance spectra of DEB-dA adducts differed from that of compound **1** (Table 1 and Figure 1). While the UV spectra of compound **2** had an absorbance maximum at neutrality of 274 nm (Figure 1B, Table 1), compounds **3** and **4** had UV absorption spectra that were nearly identical to each other and were characterized by a maximum at 264 nm (Figure 1C,D and Table 1). Under low pH conditions, the UV absorption maximum of compound **2** underwent a 6 nm hypsochromic shift, probably a result of protonation of the N-1 position of adenine (Table 1 and Figure 1B). This is similar to the pH dependence of the UV spectra reported for known N^6-substituted deoxyadenosines (*41*). No such shift was observed for compounds **3** and **4**. Instead, the UV spectra of compounds **3** and **4** were transformed at a high pH, with the development of a broad shoulder between 280 and 320 nm (Figures 1C and D). This UV absorption behavior is characteristic for 1,N^6-substituted deoxyadenosines (*41*−*44*). Taken together, the UV spectroscopy data were consistent with N^6 substitution of adenine in compound **2** and 1,N^6-susbstitution in compounds **3** and **4**.

Further insight into the structures of novel exocyclic DEB-dA lesions was obtained from tandem mass spectrometry experiments. The MS/MS fragmentation patterns of compounds **2**, **3**, and **4** under ESI$^+$-MS/MS conditions were similarly predominated by the neutral loss of deoxyribose (*m*/*z* 338.3 → 222.2 [M + 2H-dR]$^+$), not allowing any insight into the structures of modified bases (results not shown). However, characteristic MS^3 fragmentation patterns were observed when the MS/MS product ions at *m*/*z* 222.2 were isolated and subjected to further fragmentation in an ion trap mass spectrometer (Figure 1, right panel). Compound **2** exhibited a major MS^3 secondary product ion at *m*/*z* 185.9 [M + 2H-dR-2H$_2$O]$^+$ (Figure 1B). In contrast, MS^3 fragmentation of compound **3** was predominated by the fragment ions at *m*/*z* 148.0 [Ade-CH$_2$ +

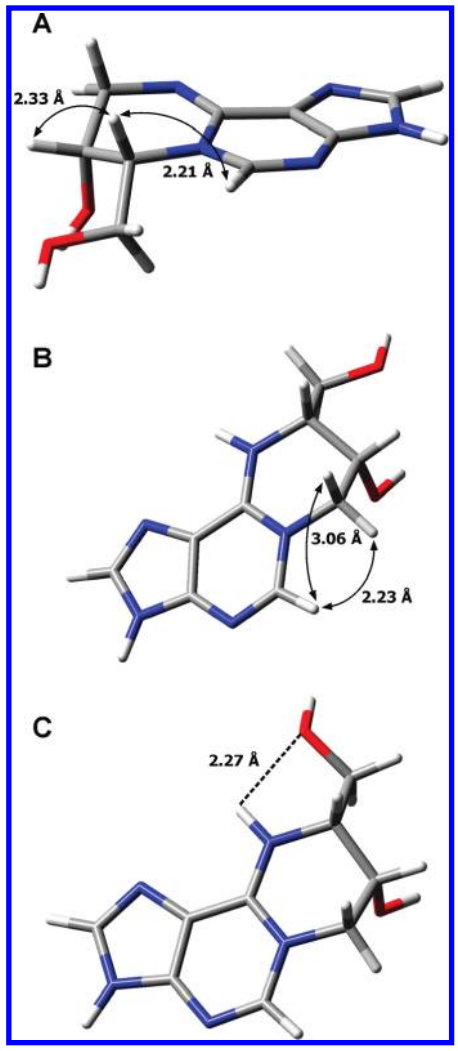

Figure 3. Molecular models of compounds **3b** (A) and **4b** (B), and proposed intramolecular hydrogen bonding in **4b** (C). Selected interatomic distances for protons observed in NOESY spectra are indicated.

H]$^+$ (Figure 1C), while the MS^3 spectrum of compound **4** was characterized by intense product ions at *m/z* 177.5 [Ade-CH-CH_2OH + H]$^+$ (Figure 1D). Our observation of different MS^3 fragmentation patterns for the three isomers of DEB-dA adducts is suggestive of significant structural differences between DEB-derived deoxyadenosine exocycles **2**, **3**, and **4**.

Periodate Oxidation Experiments to Establish the Structure of DEB-Derived Butanediol Linker. The structure of the DEB-derived side chain in compounds **2**, **3**, and **4** was explored by periodate oxidation. To simplify the experiment, periodate oxidation was conducted with free bases of **2a**, **2b**, **2c**, **3**, and **4** obtained by acid hydrolysis of the corresponding nucleosides (Chart 2). These experiments (Supporting Information Figure S-2) revealed the presence of a vicinal diol functionality in compounds **2a**, **2b**, and **2c**, consistent with the 1,4-butandiyl-2,3-diol structure of the DEB-derived exocycle (Chart 2). In contrast, the lack of periodate reactivity toward compounds **3** and **4** indicates that they do not contain a 1,2-diol functionality (Supporting Information Figure S-2). As described below, these results were subsequently confirmed by an independent synthesis of **2**, **3**, and **4**.

Structural Characterization of Compound 2 by NMR Spectroscopy. Further details of the molecular structure of compounds **2**, **3**, and **4** were obtained from one- and two-dimensional NMR spectroscopy experiments. To simplify the NMR signal assignment, the deoxyribose group of each nucleoside was cleaved in the presence of acid. NMR signal interpretation for the resulting nucleobase adducts (Chart 2) was facilitated by comparison with known ^{1}H NMR spectra of monoalkylated adenines (*45*−*48*) and 1,N^6-exocyclic dA adducts of BCNU, vinyl chloride, and α,β-unsaturated aldehydes (*10, 42, 49*).

The aromatic region of the ^{1}H NMR spectra recorded for the compounds **2a-base**, **2b-base**, and **2c-base** was characterized by signals at 8.15 ppm (H-2 of Ade) and 8.05 ppm (H-8 of Ade). The signal of N^9-H was observed at 12.88−12.89 ppm (Supporting Information Figures S-6A, S-8, and S-9). These chemical shifts are comparable to those reported for other N^6-alkyladenines (*47, 50*). However, unlike singly substituted N^6-dA derivatives, which exhibit a one-proton signal at ∼8 ppm corresponding to the exocyclic amino group, spectra of compounds **2a-base**, **2b-base**, and **2c-base** lacked the N^6-H proton signal, consistent with bis-alkylation of the N^6 position of adenine. ^{13}C chemical shifts of the aromatic part of the molecule were similar to those reported for other N^6-alkyladenines (*45, 51*). NMR spectra of compounds **2a-base** and **2b-base** were identical, consistent with their enantiomeric relationship. The presence of the pyrrolidine-2,3-diol group was supported by HSQC spectra that exhibited two methylene and two methine protons within the side chain, the TOCSY spectra that revealed strong correlations between CH_2^{α} and CH^{β} protons, CH^{β} and CH^{γ} protons, and CH_2^{δ} and CH^{γ} protons, ^{1}H NOESY experiments (Supporting Information Figure S-6), and by comparison of the NMR spectra of compound **2** with those of other pyrrolidine derivatives (*52*). No detectable correlations between the purine heterocycle and the pyrrolidine moiety of the molecule were detected in the gHMBC experiments (Supporting Information Figure S-7), as is often the case for N^6-substituted adenines (*20, 31, 53*). On the basis of NMR, MS, and periodate oxidation experiments, compounds **2a** and **2b** were identified as the enantiomers of N^6,N^6-(2,3-dihydroxybutan-1,4-diyl)-2′-deoxyadenosine (Chart 1). Similar NMR results, with a few small differences in chemical shifts, were noted for compound **2c-base** (Supporting Information Figure S-9). On the basis of the NMR, UV, and mass spectra, as well as periodate oxidation results (Supporting Information Figure S-2), compound **2c-base** was identified as *meso*-N^6,N^6-(2,3-dihydroxybutan-1,4-diyl)-adenine (Chart 2).

Final structural assignments of compounds **2a**, **2b**, and **2c**, including their absolute configurations, were made by comparing their NMR, UV, optical rotation, and mass spectra to those of authentic *R*,*R*-, *S*,*S*-, and *meso*-N^6,N^6-DHB-dA prepared independently. This stereospecific synthesis was accomplished by coupling 2′-deoxyinosine with optically pure 3*S*,4*S*-, 3*R*,4*R*-, and *meso*-pyrrolidine-3,4-diols. For example, protected *3R*,4*R*-pyrrolidine-3,4-diol **8** was synthesized from D-tartaric acid **6** as described previously (Scheme 2) (*37, 38*). Following debenzylation of **8**, the resulting *3R*,4*R* pyrrolidine-3,4-diol **9** was coupled to 2′-deoxyinosine in the presence of DMSO, DIPEA, and PyBOP (*39*) to give optically pure compound **2a** in 72% yield. The same synthetic route starting with L-tartaric acid and *meso*-tartaric acid was used to obtain optically pure compounds **2b** and **2c**, respectively. We found that the HPLC retention times, UV, NMR, and mass spectra of the independently prepared *R*,*R*-, *S*,*S*-, and *meso*-N^6,N^6-DHB-dA were identical to those of compounds **2a**, **2b**, and **2c** derived from N^6-HEB-dA (Scheme 1), confirming their chemical structures as *S*,*S*-, *R*,*R*-, and *meso*-N^6,N^6-(2,3-dihydroxybutan-1,4-diyl)-2′-deoxyadenosine, respectively (Chart 1).

Scheme 3. Protonated and Deprotonated Forms of 3 and 4

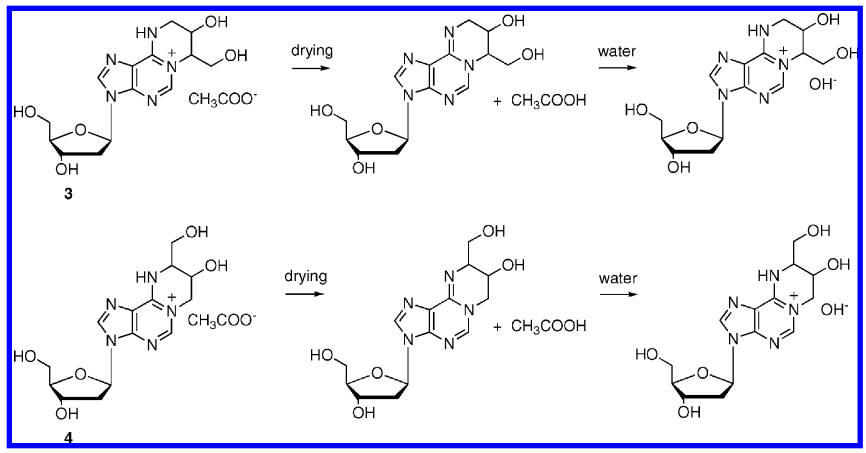

Scheme 4. Stereospecific Synthesis of Compounds 3a, 3b, 4a, and 4b[a].

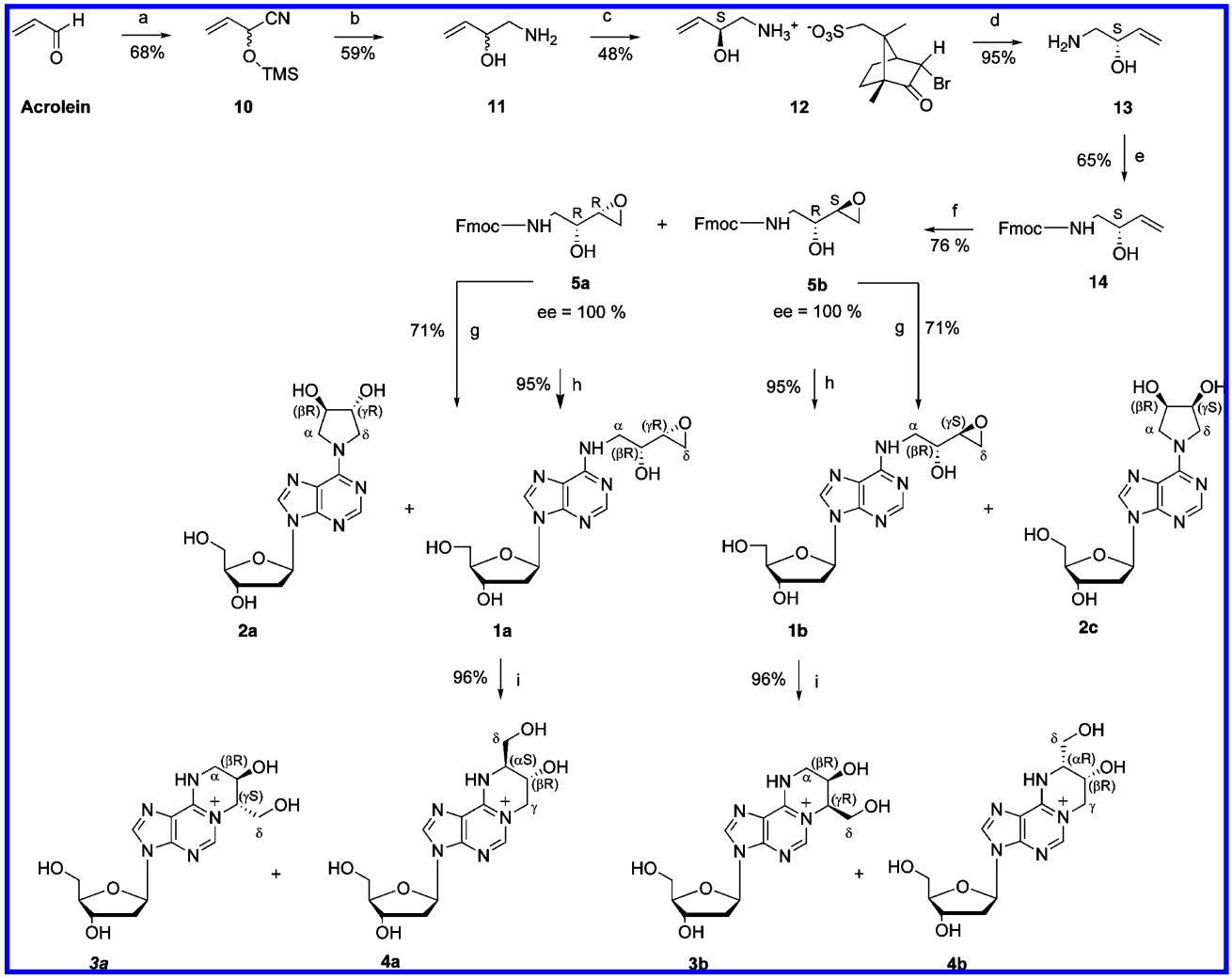

[a] (a) TMS-CN, Zn−I_2, reflux; (b) (i) $LiAlH_4/Et_2O$; (ii) aq. work up; (c) 1*R-endo*,*anti*-(+)-3-bromocamphor-8-sulfonic acid ammonium salt, methanol; (d) aq., excess $Ba(OH)_2$; (e) Fmoc-Cl, aq. dioxane, aq. Na_2CO_3, rt; (f) (i) *m*CPBA, CH_2Cl_2, rt, 18 h; (ii) HPLC separation of diastereomers; (g) 6-chloropurine-2′-deoxyriboside, DIPEA, DMSO, 37 °C, 3 d; (h) 2′-deoxyinosine, PyBOP, DMSO, DIPEA, rt, 5 d; (i) H_2O, rt, 15 h.

As noted above, the NMR spectra of compound **2-base** recorded at an ambient temperature (25 °C) reveal separate signals for the two methylene protons (CH_2^{α} and CH_2^{δ}) and for the two methine protons of the pyrrolidine-3,4-diol moiety (CH^{β} and CH^{γ}). Similarly, ^{13}C NMR signals of carbons β and γ, as well as those of carbons α and δ, have slightly different chemical shifts (Supporting Information Figure S-6B). This is in contrast with the fully symmetrical ^{1}H and ^{13}C spectra of synthetic pyrrolidine-3,4-diols prior to their coupling with the purine heterocycle (Figures S-4 and S-5 in Supporting Information). This discrepancy can be explained by a hindered rotation about the C6−N6 bond in compound **2**, resulting in a distinct stereoelectronic environment for carbons and hydrogens located on the opposite sides of the pyrrolidine ring (e.g., CH_2^{α} and

Scheme 5. Dimroth Rearrangement of Compound 3 to Form 4

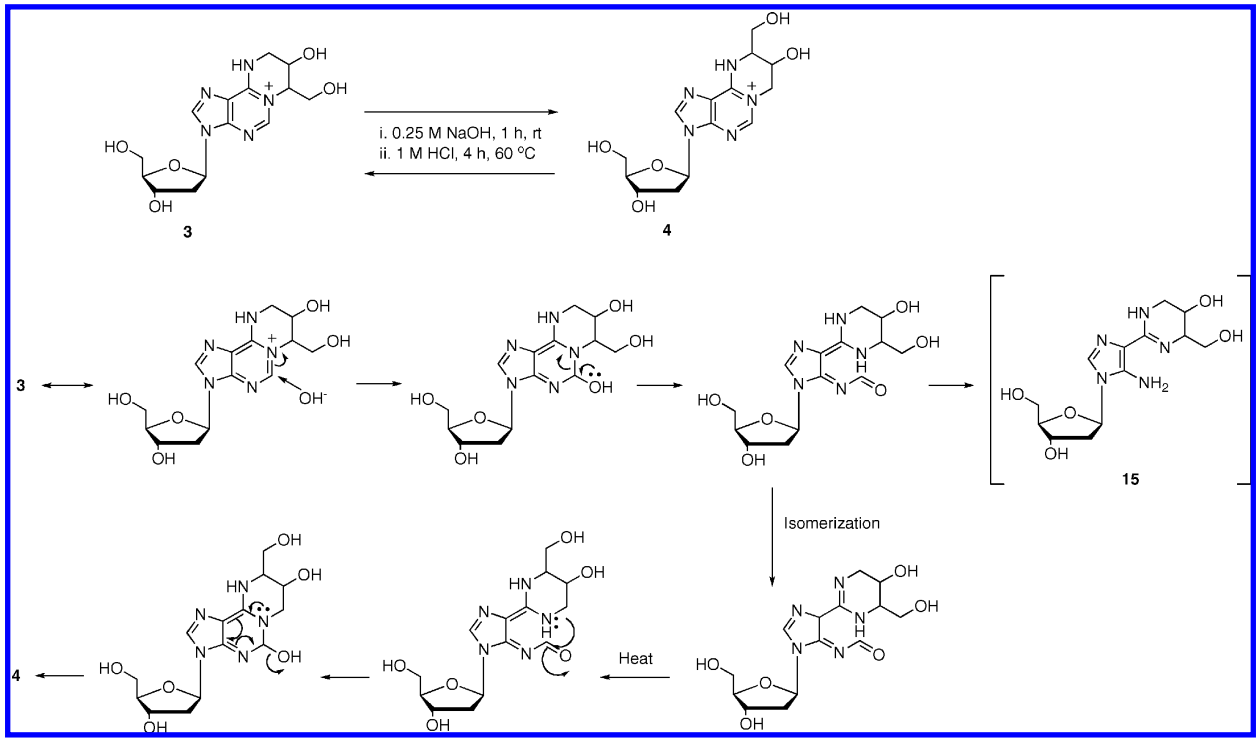

CH^{β} versus CH^{γ} and $CH_2{}^{\delta}$). This hypothesis is fully supported by density functional calculations that reveal that the lone electron pair of the pyrrolidine nitrogen is shared with the π-electron system of the purine ring, resulting in a partial double bond character for the C6−N6 bond. Conformational analyses (Supporting Information Figures S-10−S-12) predict that the barrier of rotation about the C6−N6 bond is between 14.5 and 17.5 kcal/mol. As a result, at room temperature, one side of the pyrrolidine ring ($CH_2{}^{\alpha}$ and CH^{β}) experiences a greater ring current and a more pronounced deshielding than does the other side (CH^{γ} and $CH_2{}^{\delta}$), leading to a downfield shift in the ^{1}H and ^{13}C NMR spectra.

To confirm the results of this computational study experimentally, temperature-dependent ^{1}H NMR spectra of compounds **2a** and **2b** were recorded. As the temperature was increased from 25 °C to 50, 65, and 85 °C, proton signals corresponding to CH^{β} and CH^{γ} merged, yielding a single two proton signal at 4.04 ppm (Supporting Information Figure S-13). Similarly, the signals corresponding to $CH_2{}^{\alpha}$ and $CH_2{}^{\delta}$ coalesced at an increased temperature, although a higher temperature (∼85 °C) was required because of a greater separation of their chemical shifts (4.21 and 4.00, and 3.69 and 3.62 ppm, respectively). Taken together, our results suggest that the bond rotation along the C6−N6 bond of compound **2** under physiological temperature is hindered, resulting in an asymmetric structure.

Structural Characterization of Compound 3: 1,N^6-(2-Hydroxy-3-hydroxymethylpropan-1,3-diyl)-2′-deoxyadenosine (Compound 3). Since compound **3** was obtained by spontaneous cyclization of compound **1** (in Scheme 1), the adenine substitution pattern of the resulting exocycle must include the N^6 position of adenine. As discussed above, the UV spectral data for **3** are indicative of the 1,N^6-dialkylation (Figure 1C). Further proof of the 1,N^6-substitution of adenine in compound **3** is obtained from gHMBC and 2-D NOESY spectra (Figure 2B,D and Supporting Information Figures S-14−S-16 and S-21). In particular, gHMBC signals are found between the C-6 of adenine and the $CH_2{}^{\alpha}$ protons of the side chain (Figure 2B), and a correlation is observed between the carbon γ of the side chain and the H-2 proton of the adenine heterocycle (Figure 2D). Furthermore, NOESY correlations are observed between the H-2 proton of the adenine nucleobase and the CH^{γ} proton of the side chain of compounds **3**, **3a**, and **3b**.

The detailed structures of compounds **3a** and **3b** were established by considering the results of two-dimensional NMR experiments. A phase-sensitive HSQC (^{1}H−^{13}C) experiment (Figure 2C) was instrumental for distinguishing between the methylene and methine protons within the DEB-derived exocycle. The diastereotopic methylene protons of the $CH_2{}^{\delta}$ group were observed as two multiplets at 3.59 and 3.39 ppm (Figure 2A). According to the HMQC and HSQC data, these two protons are attached to the same carbon atom (61.9 ppm, Supporting Information Figure S-12). These two protons couple with each other in the COSY and NOESY spectra, confirming their geminal nature. Furthermore, the $CH_2{}^{\delta}$ group is connected to a hydroxyl based on the results of COSY experiments (Supporting Information Figure S-14). Taken together with the results of periodate oxidation (Supporting Information Figure S-2), these data establish the structure of **3** as 1,N^6-(2-hydroxy-3-hydroxymethylpropan-1,3-diyl)-2′-deoxyadenosine (Chart 1).

This structural assignment is supported by comparing the NMR and UV data of compound **3** with those published for other 1,N^6-dA exocyclic compounds, e.g., 1,N^6-(propano)-2′-deoxyadenosine (*53*) and 1,N^6-(2-hydroxypropano)-2′-deoxyadenosine (*43*). Density functional calculations predict that the distance between H-2 and CH^{γ} protons in 1,N^6-(2-hydroxy-3-hydroxymethylpropan-1,3-diyl)-2′-deoxyadenosine is 2.21 Å (Figure 3A), consistent with the NOESY results discussed above.

Despite the single substitution of the exocyclic amino group in compound **3**, no ^{1}H NMR signal corresponding to the exocyclic NH proton is observed (Figure 2A). Other N1-alkyladenines are known to be positively charged in aqueous solutions at a neutral pH (the pK_a of 1-methyladenine is 8.25) (*45*), with the charge localized mainly at the N1 position. HPLC behavior of compounds **3** and **4**, e.g., their poor retention on reversed phase HPLC columns in the absence of ion pairing reagents, but strong retention on cation exchange columns at

pH 7, suggests that they are charged species under aqueous conditions, containing a proton at the N^6 and a double bond between the C6 and the N1 (Scheme 3). Further support for the presence of a positive charge on the N-1 under aqueous conditions is obtained from the downfield shifts of the NMR signals of H-2, C-2, and C-6 compared to the corresponding signals in dA. The proton NMR signal of H-2 in **3** is shifted downfield by 0.6 ppm when the spectrum is recorded in D_2O relative to that in dry DMSO (Figure S-25 in Supporting Information). This shift is greater than can be accounted for by solvent effect and is consistent with the presence of a positive charge when compound **3a** is dissolved in water. This NMR behavior is analogous to that of structurally similar 1,N^6-dA exocyclic adducts containing a positive charge on the N-1 (*43*). We hypothesize that NMR sample drying under high vacuum conditions leads to deprotonation of the N^6-H (and the removal of acetic acid) and the formation of the N6−C6 double bond (Scheme 3), explaining the absence of the N^6-H proton signal in the ^{1}H NMR spectrum of compound **3a** (Figure 2A).

Structural Characterization of Compound 4: 1,N^6-(1-Hydroxymethyl-2-hydroxypropan-1,3-diyl)-2′-deoxyadenosine (Compound 4). The UV spectroscopy results for compound **4** discussed above (Figure 1 and Table 1) are consistent with the 1,N^6-ring substitution pattern, while periodate oxidation experiments establish the absence of a vicinal diol functionality (Supporting Information Figure S-2). Furthermore, UV absorbance spectra (Figure 1) and the downfield regions of the ^{1}H NMR spectra of compound **4** (Supporting Information Figures S-17 and S-18) are identical to those of compound **3**, suggesting that they have the same adenine ring substitution patterns. However, our observation of distinct MS^3 spectra and significant differences within the upfield regions of the ^{1}H NMR spectra of compounds **3** and **4** (see Figure 1C and D (right panel) and Supporting Information Figures S-17 and S-18) suggests that they have different side chain structures.

Two-dimensional NMR experiments were used to establish the exact connectivity between the adenine heterocycle and the DEB-derived side chain in compound **4**. In particular, NOESY correlations between the H-2 adenine proton and both CH_2^{γ} protons within the propano exocycle were observed (Supporting Information Figures S-17 and S-18). Furthermore, HMBC correlations were detected between the two CH_2^{γ} protons (3.95 and 3.80 ppm) and the C-2 carbon of adenine (148.6 ppm) of **4a**, strongly suggesting that a terminal methylene group of DEB is connected to the N-1 position of adenine (Supporting Information Figure S-17). On the other side, the N^6 position of adenine is bound to an internal carbon of DEB as indicated by the presence of the HMBC correlation between the CH^{α} proton (3.48 ppm) and the C-6 carbon atom of the nucleobase (142.3 ppm) (Supporting Information Figures S-17 and S-18). Taken together, these results are consistent with the structure of 1,N^6-(1-hydroxymethyl-2-hydroxypropan-1,3-diyl)-2′-deoxyadenosine for compound **4**. According to our density functional calculations, the distances between the H-2 of adenine and the two γ methylene protons in 1,N^6-(1-hydroxymethyl-2-hydroxypropan-1,3-diyl)-2′-deoxyadenosine are 2.23 and 3.06 Å, respectively (Figure 3B below), consistent with the NOESY results for compound **4** (Supporting Information Figures S-17 and S-18).

Stereospecific Synthesis of Compounds 3a, 3b, 4a, and 4b and the Assignment of Their Absolute Configuration. In order to establish the absolute configuration of compounds **3a**, **3b**, **4a**, and **4b**, stereospecific synthesis of each isomer was required. In our synthetic scheme, racemic 1-aminobut-3-ene-2-ol **11** was derived from the addition of trimethylsilyl cyanide to acrolein to generate a protected cyanohydrin **10**, which was subjected to reduction with lithium aluminum hydride (Scheme 4) (*30, 31*). The racemic mixture of 1-amino-3-butene-2-ols **11** was separated by diastereomeric resolution following derivatization with sodium [(1*R*)-(*endo*, *anti*)]-(+)-3-bromocamphor-8-sulfonic acid ammonium salt to give crystals of **12** (Scheme 4) (*32, 33*). The absolute configuration of the derivatized 1-amino-3-butene-2-ol **12** (*S*), was established by X-ray crystallography (Supporting Information Figure S-20). Following crystal isolation, (*S*)-1-aminobut-3-ene-2-ol **13** was regenerated by alkaline hydrolysis. Fmoc-protected 1-aminobut-3-ene-2-ol **14** was subjected to epoxidation in the presence of *m*CPBA to give diastereomeric 1-amino-3,4-epoxybut-2-ols **5a** and **5b** (*30*), which were resolved by preparative HPLC (Scheme 4). The other two isomers (**5c** and **5d** in Chart 1) were obtained analogously using (*R*)-1-aminobut-3-ene-2-ol isolated from the mother liquor following the crystallization of **12**, followed by alkaline hydrolysis.

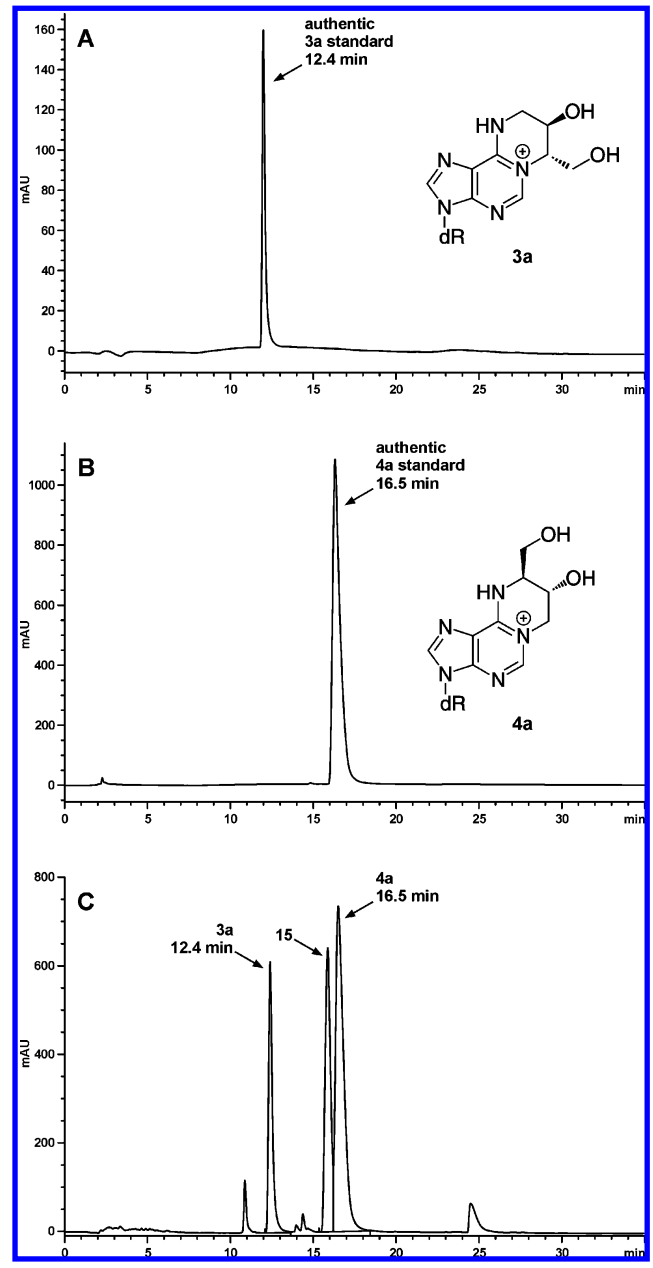

Figure 4. HPLC-UV analysis of pure standard of **3a** (A), pure standard of **4a** (B), and the reaction mixture following forced Dimroth rearrangement of **3a** (C).

Scheme 6. Formation of Stereoisomers of 3 and 4 in Animals Treated with 1,3-Butadiene

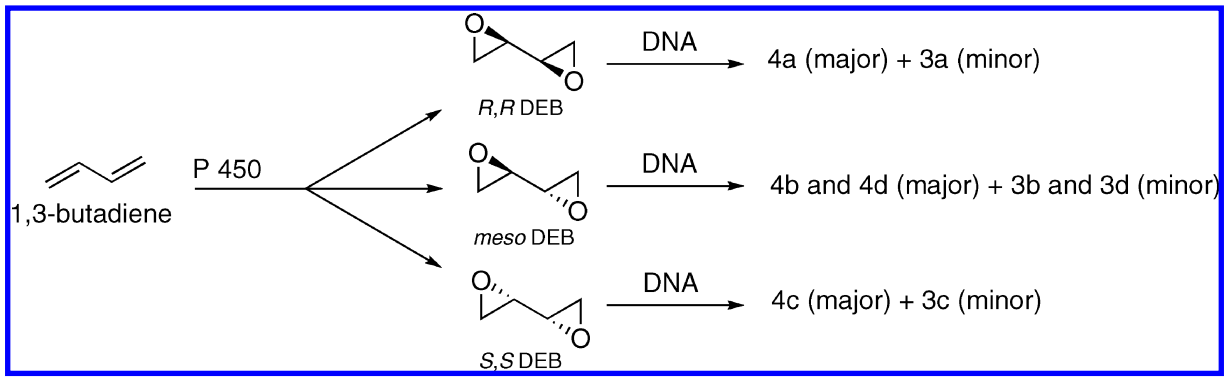

Two sets of coupling conditions were tested for the coupling of Fmoc-protected 1-amino-3,4-epoxybut-2-ols with the purine heterocycle. Coupling of **5a** with 6-chloropurine-2′-deoxyriboside for 3 days in the presence of DIPEA gave compound **1a** with 71% maximum yield (Scheme 4). An improved yield of **1a** (95%) was achieved by coupling of **5a** with 2′-deoxyinosine in the presence of PyBOP for 5 days (*39*). Optically pure compounds **3a** and **4a** were obtained by spontaneous cyclization of **1a** in water overnight at 25 °C, followed by reversed phase HPLC purification (Scheme 4). Analogous reactions of **5b** produced monoepoxide **1b**, which cyclized to compounds **3b** and **4b** (7:3 molar ratio by HPLC). Further experiments indicated that compounds **3a** and **3b** can be generated selectively in a 98% yield when the cyclization time is decreased to 3 h. Interestingly, the stereochemistry of the oxirane ring in **1a** and **1b** did not affect their cyclization kinetics ($t_{1/2}$ at 37 °C in water was ∼58 min for both isomers; see Supporting Information Figure S-19).

The absolute configurations of stereogenic centers within the propano group of compound **3a** (β and γ in Chart 1) were assigned as follows. The configuration at the β position of **3a** should be *R* because it is obtained by the cyclization of **1a**, which has the $\beta R,\gamma R$ stereochemistry (Scheme 4), and the β stereocenter is unchanged in this reaction. In contrast, the optical configuration of the γ carbon is inverted as a result of S_N2 type nucleophilic substitution at this position, resulting in the *S* stereochemistry (Scheme 4). This assignment is experimentally confirmed by the lack of spacial correlations between the β and the γ protons in the NOESY NMR spectrum of **3a** (Supporting Information Figure S-15). Similarly, the chiral centers within the propane moiety of **3b** were assigned as $\beta R,\gamma R$ because it was obtained by intramolecular nucleophilic substitution of $\beta R,\gamma S$-1-amino-2-hydroxy-3,4-epoxybutane **1b**, which was experimentally confirmed by the presence of NOESY NMR signals between the β and γ protons of **3b** (Supporting Information Figure S-16). Density functional calculations predict that the distance between β and γ protons in $\beta R,\gamma R$-*1*,N^6-(2-hydroxy-3-hydroxymethylpropan-1,3-diyl)-2′-deoxyadenosine is between 2.3−2.4 Å, depending on the conformation of the γ-hydroxymethyl group (Figure 3A), corroborating the observed NOESY correlations and supporting the stereochemical assignment of **3b**.

The absolute stereochemistry of compound **4a** was assigned as $\alpha S,\beta R$ on the basis of the mechanism of its formation via the isomerization of **3a** (see below) and the absence of the NOE correlations between the β and α protons (Supporting Information Figure S-17). Similarly, compound **4b** was assigned the $\alpha R,\beta R$ configuration, supported by the observation of NOE correlations between the β and α protons of **4b** and density functional calculations (Figure 3B and Supporting Information Figure S-18).

Compounds **1c** and **1d** and their cyclization products **3c**, **4c**, **3d**, and **4d** (Chart 1) were generated analogously starting with **5c** and **5d**, respectively.

Solvent-Dependent Regioselectivity for the Cyclization of Compound 1. As discussed above, compound **1** spontaneously cyclizes to form the corresponding 1,N^6 exocyclic compound **3** when allowed to incubate in water under physiological pH (Scheme 1). In contrast, the N^6,N^6 exocycle **2** is not observed when **1** is allowed to cyclize in an aqueous solution. Instead, **2** becomes a significant side product from the coupling reaction of 6-chloropurine-2′-deoxyriboside with 1-amino-3,4-epoxybut-2-ol when the coupling time is extended to > 3 days (Scheme 1, Supporting Information Figure S-3). The same product **2** is generated when purified **1** is incubated under our standard coupling conditions (DMSO in the presence of DIPEA) (Scheme 1).

Taken together, these results indicate that the regioselectivity of the cyclization of compound **1** is determined by solvent identity. Under aqueous conditions, **1** spontaneously cyclizes to **3**, while **2** is preferentially formed in an aprotic solvent (DMSO) in the presence of organic base (Scheme 1). These results can be explained by the altered nucleophilicity of the N^6 and the *N*1 of **1** under these two sets of conditions, likely a result of N^6H deprotonation in an aprotic solvent in the presence of *N*,*N*-diisopropylethyl amine.

Forced Dimroth Rearrangement of Compound 3 to Compound 4. While the formation of compound **3** from compound **1** can be explained by intramolecular nucleophilic substitution (Scheme 1), no such mechanism can be proposed for compound **4**. Kinetic analyses indicate that **3** originates directly from **1** but that there is a delay in the formation of **4**, which requires extended incubation times (Supporting Information Figure S-22). We hypothesized that compound **4** is formed from **3** by a base-catalyzed Dimroth rearrangement (Scheme 5). To test this hypothesis, **3a** was subjected to forced Dimroth rearrangement in aqueous NaOH (*54*). Capillary HPLC analysis of the reaction mixture revealed the presence of compounds **3a** and **4a** in a 3:7 molar ratio (Figure 4C). Interestingly, the same product ratio was observed when purified **4a** was subjected to forced Dimroth rearrangement (not shown).

An additional nucleoside product **15** was observed while analyzing the reaction mixture from Dimroth rearrangement by capillary HPLC. It was tentatively assigned the structure of 2-(5-amino-1-(2-deoxy-β-D-*erythro*-pentofuranosyl)-imidazol-4-yl)-4-(hydroxymethyl)-tetrahydropyrimidin-5-ol (compound **15** in Supporting Information Figure S-24) on the basis of its UV absorption spectra (λ_{max} = 284 nm) and MS/MS fragmentation pattern. We hypothesized that this compound was produced by

a hydroxyl ion attack on compounds **3** or **4**, followed by a loss of CO as proposed by Sugiyama et al. for structurally related compounds (*55*).

To determine whether Dimroth rearrangement of compounds **3** and **4** can take place under mild conditions, purified compounds **3a** and **4a** were individually dissolved in water and incubated at room temperature or at 37 °C for up to 5 days. The rearrangement products were detected by HPLC-ESI$^+$-MS/MS (Supporting Information Figure S-23). We observed a slow conversion of **3a** to **4a** at room temperature (12% in 5 days) and a faster rearrangement at 37 °C (66% in 5 days). In contrast, the formation of **3a** from **4a** was inefficient under both conditions (only 20% at 37 °C in 5 days). Irrespective of the temperature, the same molar ratio (70% of **4a** and 30% of **3a**) was observed when either **3a** or **4a** was allowed to equilibrate in water for a sufficient time (16 days). Kinetic analyses of this conversion (Supporting Information Figure S-23) reveal that the half-lives for the conversion of **3a** → **4a** and **4a** → **3a** are 71.5 and 365 h, respectively. Taken together, these results indicate that **4a** and **3a** can be interconverted under physiological pH, with the equilibrium shifted toward **4a** as a more thermodynamically stable product. Density functional calculations support this finding as compound **4a** is 1.9 kcal/mol lower in energy than **3a**. We hypothesize that the additional stability of **4a** is derived mainly from the formation of an intramolecular hydrogen bond between between the N^6-H and the hydroxymethyl oxygen of the exocycle (Figure 3C).

Detection of Exocyclic DEB-dA Adducts in DEB-Treated DNA and in Liver DNA of BD Exposed Mice. To establish whether exocyclic DEB-dA adducts **2**, **3**, and **4** are biologically relevant, aliquots of double stranded DNA (calf thymus DNA) were separately treated with *S*,*S*-, *R*,*R*-, or *meso*-DEB (Scheme 6). All three isomers of DEB were employed in order to investigate the potential effects of diepoxide chirality on exocyclic DEB-dA adduct formation. The resulting alkylated DNA was enzymatically digested to deoxynucleosides, spiked with $^{15}N_4$-labeled compounds **3** and **4** (internal standards for mass spectrometry), and purified by solid phase extraction. HPLC-ESI$^+$-MS/MS analysis of samples treated with *R*,*R*-DEB revealed two major peaks eluting at 12.4 and 17.7 min (Figure 5A), which were identified as compounds **3a** and **4a**, respectively, on the basis of their MS^3 fragmentation patterns and HPLC retention times. Similar results were obtained for *S*,*S*-DEB (Figure 5B) since compounds **3c** and **4c** originating from *S*,*S*-DEB have the same HPLC retention times as **3a** and **4a**, respectively. Samples treated with *meso*-DEB revealed HPLC-ESI-MS/MS signals at 19.2 and 21.3 min, corresponding to compounds **4b/4d** and **3b/3d**, respectively. In all of the cases, the amounts of compound **4** were greater than that of compound **3**. In contrast, compound **2** was not found in DNA hydrolysates, although small amounts were detected in a separate experiment using >200 molar excess of DEB (results not shown).

The amounts of compounds **3** and **4** present in DNA hydrolysates were calculated from HPLC-ESI-MS/MS peak areas corresponding to the analytes and the corresponding internal standards. As shown in Figure 5D, concentrations of exocyclic 1,N^6-HMHP-dA adducts increased linearly as the concentration of DEB was gradually raised from 50 to 1000 μM. Similar numbers of exocyclic DEB-dA adducts were observed in DNA treated with *S*,*S*-, *R*,*R*-, or *meso*-DEB, suggesting that the DEB isomers are equally capable of inducing exocyclic adenine lesions in DNA. This is in contrast with our earlier results for DNA cross-linking by DEB isomers, which revealed that the *S*,*S* isomer formed the highest numbers of interstrand guanine−guanine lesions, while *meso*-DEB induced equal numbers of intrastrand and interstrand *bis*-N7G-BD lesions (*21*).

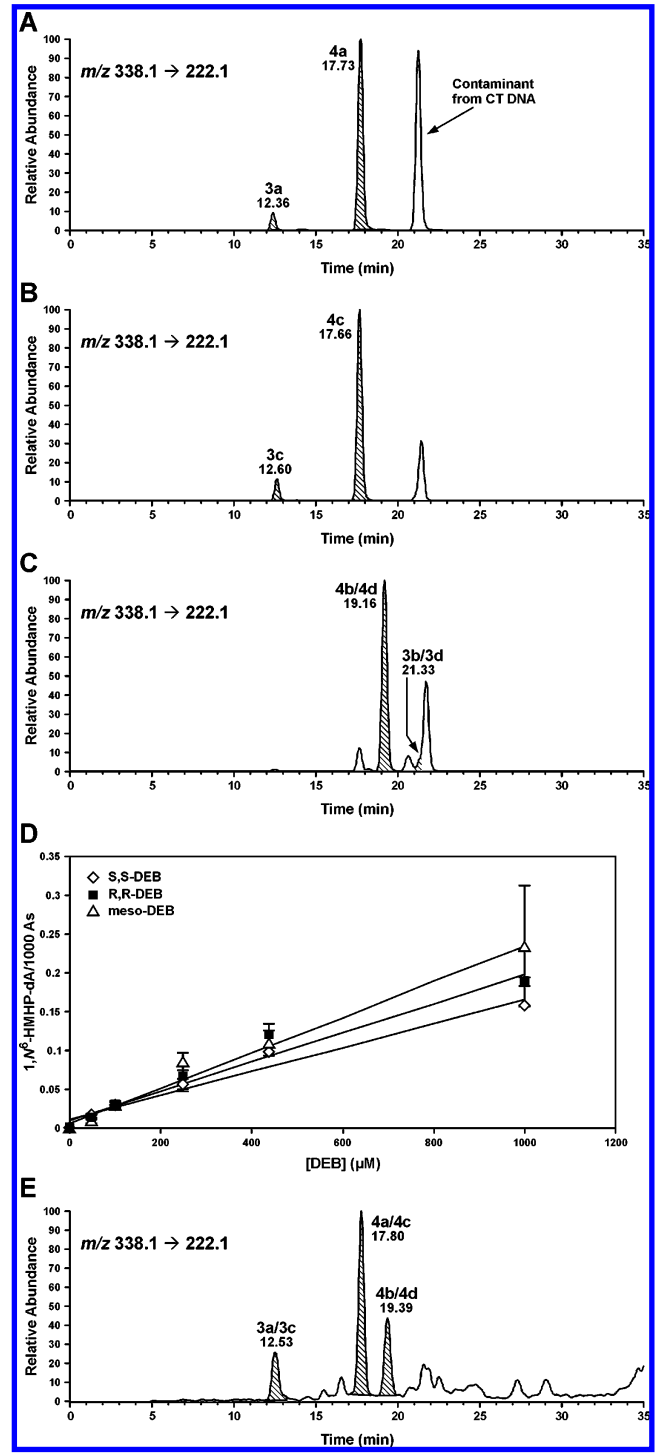

Figure 5. Formation of exocyclic DEB-dA adducts in DNA in vitro and in vivo: capillary HPLC-ESI$^+$ MS/MS analysis of compounds **3** and **4** in enzymatic digests of calf thymus DNA treated with *R*,*R* DEB (A); *S*,*S* DEB (B); and *meso* DEB (250 μM DEB, 24 h at 37 °C) (C); concentration-dependent formation of exocyclic DEB-dA adducts **3** and **4** in calf thymus DNA treated with 0−1 mM DEB (24 h at 37 °C) (D); and capillary HPLC-ESI$^+$ MS/MS analysis of **3** and **4** in enzymatic digests of liver DNA from a B6C3F1 mouse exposed to 625 ppm butadiene for 2 weeks (E). No signals corresponding to **3** and **4** were observed in DNA digests from control animals.

Adducts **3** and **4** were also present in genomic DNA isolated from the liver of laboratory mice exposed to 1,3-butadiene by inhalation (Figure 5E). Compounds **4a/4c** (61%) were the most

Scheme 7. Proposed Mechanism for the Formation of 3 and 4 in DEB-Treated DNA under Physiological Conditions

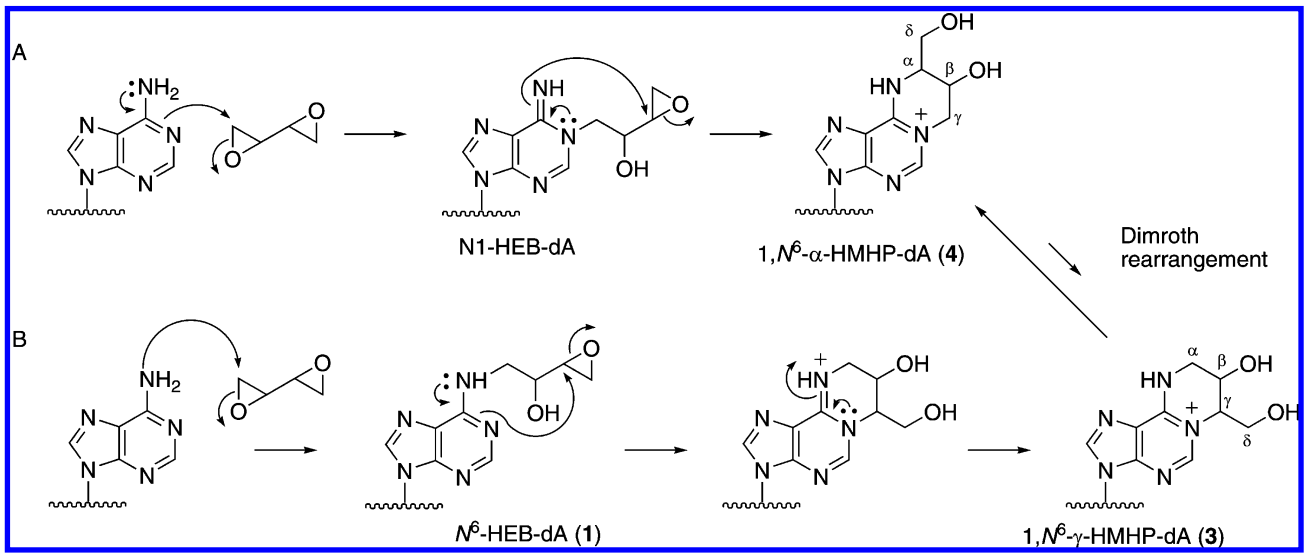

Scheme 8. Pericyclic Rearrangement for the Interconversion of 4a and 3a under Physiological Conditions

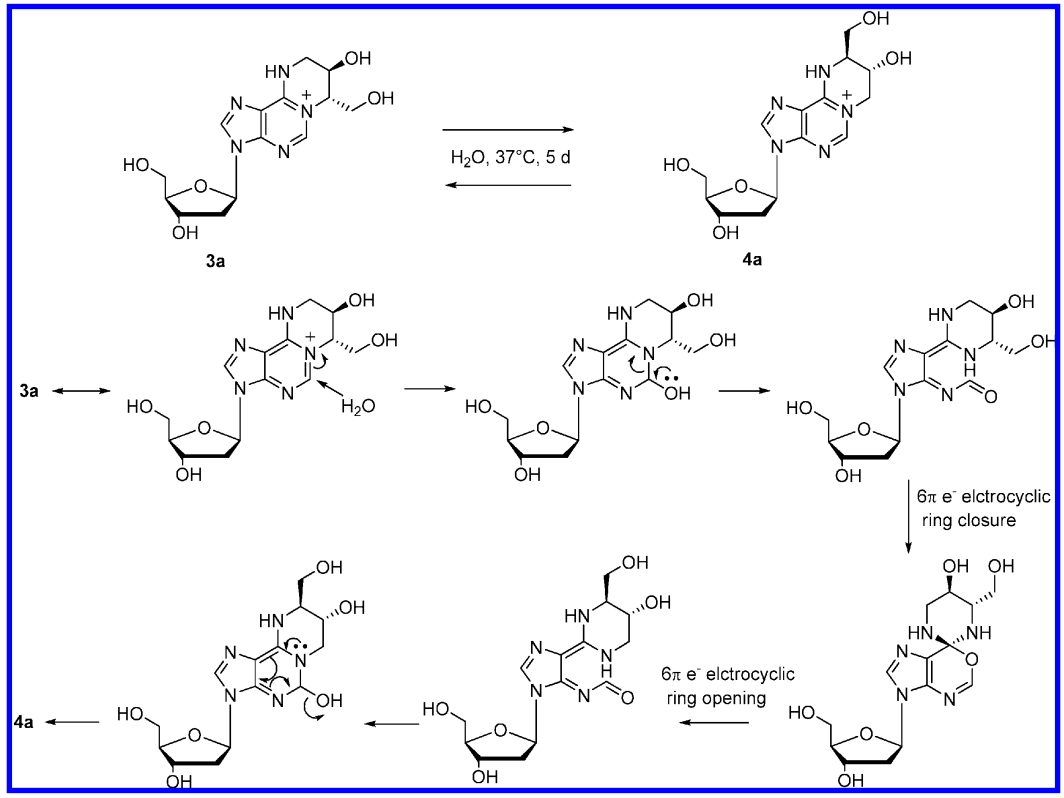

abundant, followed by **4b/4d** (27%) and **3a/3c** (12%) (the individual isomers of **4a/4c** and **3a/3c** are not resolved under our HPLC conditions). The presence of stereoisomers of **3** and **4** in vivo is consistent with nonstereoselective metabolic activation of 1,3-butadiene to *S*,*S*-, *R*,*R*-, and *meso*-DEB (Scheme 6) (*14*). As previously observed for guanine−guanine cross-links of DEB (*40*), exocyclic dA adducts originating from *S*,*S*+*R*,*R*-DEB (**3a**, **4a**, **3c**, **4c**) are more abundant than the corresponding lesions of *meso*-DEB (**3b**, **4b**, **3c**, **4c**, see Scheme 6 and Figure 5E). This may be explained by the greater amounts of *S*,*S*- and *R*,*R*-diepoxides produced upon metabolic activation of BD as compared with that of *meso*-DEB. Studies using cDNA-expressed human P450 monooxygenases have shown that individual P450s can generate meso and racemic DEB in different molar ratios (*56*). In particular, P450 2A6 and 2E1 favor meso over racemic DEB, whereas 2C9 forms equal levels of each (*56*). Alternatively, mice may detoxify *meso*-DEB at a faster rate than racemic DEB. For example, epoxide hydrolase (EH), an enzyme that detoxifies DEB by hydrolyzing the epoxide ring to a diol, has been reported to hydrolyze *meso*-DEB at a faster rate than *S*,*S*- and *R*,*R*-diepoxides (*56*), potentially leading to smaller amounts of *meso*-DEB available for reactions with DNA.

Taken together, our results indicate that the major exocyclic DEB-dA adducts produced following in vitro or in vivo exposure of DNA to DEB have the structures of 1,N^6-(1-hydroxymethyl-2-hydroxypropan-1,3-diyl)-2′-deoxyadenosine (compound **4**) and 1,N^6-(2-hydroxy-3-hydroxymethylpropan-1,3-diyl)-2′-deoxyadenosine (compound **3**). Although the amounts of adducts **3** and **4** in the liver DNA following exposure to 1,3-butadiene are significantly lower than the numbers of DEB-induced DNA−DNA cross-links, 1,4-*bis*-(guan-7-yl)-2,3-butanediol (*bis*-N7G-

BD), and 1-(guan-7-yl)-4-(aden-1-yl)-2,3-butanediol (N7G-N1A-BD) (the molar ratio of *bis*-N7G-BD/N7G-N1A-BD/ adducts **3** and **4** is 1:0.08:0.03), exocyclic DEB-dA lesions are hydrolytically stable and may persist in vivo. Indeed, our recent studies indicate that **3** and **4** are present in mouse liver at least 2 weeks following exposure (Goggin, M., and Tretyakova, N., manuscript in preparation). Compounds **3** and **4** are not substrates for base excision repair or nucleotide excision repair, leading to their potential accumulation in target tissues (Goggin, M., and Tretyakova, N., manuscript in preparation). On the basis of these observations, we hypothesize that compounds **3** and **4** play an important role in the mutagenicity and carcinogenicity of 1,3-butadiene.

Concluding Remarks. Our results presented above are the first report for the formation of potentially promutagenic exocyclic DEB-dA lesions, which have the structures of N^6,N^6-(2,3-dihydroxybutan-1,4-diyl)-2′-deoxyadenosine (compound **2**), 1,N^6-(1-hydroxymethyl-2-hydroxypropan-1,3-diyl)-2′-deoxyadenosine (compound **4**), and 1,N^6-(2-hydroxy-3-hydroxymethylpropan-1,3-diyl)-2′-deoxyadenosine (compound **3**). The structural identities and optical configurations of the novel nucleosides were confirmed by an independent stereospecific synthesis. We hypothesize that in DNA under physiological conditions, DEB alkylates the N-1 position of adenine in DNA to form N1-(2-hydroxy-3,4-epoxybut-1-yl)-adenine adducts, which undergo spontaneous intramolecular nucleophilic substitution to yield compound **4** (Scheme 7A). The minor regioisomer **3** is formed either by alkylation of the N^6 of adenine bases by DEB, followed by cyclization (Scheme 7B), or by Dimroth-like rearrangement of **4** (Scheme 5). Compounds **3** and **4** are interconverted under physiological conditions by a reversible reaction favoring **4** as a more stable thermodynamic product. While Dimroth rearrangement is expected to be slow at physiological pH, an alternative mechanism based on low energy unimolecular pericyclic reactions (*57*) may explain the formation of **4** from **3** (Scheme 8).

Compounds **4a/4c** were the most abundant exocyclic DEB-dA adducts observed in DEB-treated DNA and also in DNA extracted from the liver tissues of laboratory mice exposed to 1,3-butadiene by inhalation. Levels of compounds **3** and **4** in DNA increased with DEB concentration, and little difference in reactivity was observed for the three isomers of DEB (Figure 5D).

While the biological significance of the novel DEB-dA lesions discovered in this work remains to be established, they may be responsible for the ability of 1,3-butadiene and DEB to induce a large number of A → T mutations (site specific mutagenesis experiments are in progress). Since Watson−Crick base-pairing of compounds **3** and **4** with dT is blocked by the (1-hydroxymethyl-2-hydroxy-1,3-propano) exocycle, the modified nucleoside is likely to adopt the syn conformation about the glycosidic bond as previously observed for 1,N^6-εdA and N1-HB-dI adducts (*4, 5, 10, 58*), preventing accurate replication. We hypothesize that the modified dA forms a Hoogsteen base pair with the incoming protonated dATP, leading to A → T transversions. The synthetic methodologies established in the present work have been recently used to generate DNA oligodeoxynucleotides containing site- and stereospecific adducts **2**, **3**, and **4** (Seneviratne, U., and Tretyakova, N., manuscript in preparation). Our ongoing studies are employing solution NMR and site-specific mutagenesis to establish the effects of the novel DEB-dA lesions on DNA structure and DNA polymerase fidelity.

Acknowledgment. We thank Kris Murphy for optimizing the yields of several key synthetic steps, Brock Matter (University of Minnesota Cancer Center) for his assistance with the HPLC and mass spectrometry experiments, Victor G. Young, Jr. (X-ray Crystallographic Laboratory, Department of Chemistry) for conducting crystallography experiments, and Bob Carlson (University of Minnesota Cancer Center) for preparing figures for this manuscript. NMR instrumentation was provided with funds from the NSF (BIR-961477), the University of Minnesota Medical School, and the Minnesota Medical Foundation. This research is supported by grants from the NCI (R01 CA095039) and the Health Effects Institute (Agreement 05-12). D.Y. is grateful for financial support provided by the National Institutes of Health (GM62248). A.M. is grateful for support through a Department of Energy NDSEG fellowship. Computational resources were provided by the Minnesota Supercomputing Institute.

Supporting Information Available: Kinetics data for cyclization and rearrangement experiments, NMR data tables, molecular modeling results, and crystallography data. This material is available free of charge via the Internet at http://pubs.acs.org.

References

(1) Blair, I. A. (2008) DNA adducts with lipid peroxidation products. *J. Biol. Chem. 283*, 15545–15549.
(2) Yang, I. Y., Hashimoto, K., de Wind, N., Blair, I. A., and Moriya, M. (2009) Two distinct translesion synthesis pathways across a lipid peroxidation-derived DNA adduct in mammalian cells. *J. Biol. Chem. 284*, 191–198.
(3) Medeiros, M. H. (2009) Exocyclic DNA adducts as biomarkers of lipid oxidation and predictors of disease. Challenges in developing sensitive and specific methods for clinical studies. *Chem. Res. Toxicol. 22*, 419–425.
(4) Nair, D. T., Johnson, R. E., Prakash, L., Prakash, S., and Aggarwal, A. K. (2006) Hoogsteen base pair formation promotes synthesis opposite the 1, N^6-ethenodeoxyadenosine lesion by human DNA polymerase ι. *Nat. Struct. Mol. Biol. 13*, 619–625.
(5) Basu, A. K., McNulty, J. M., and McGregor, W. G. (1999) Solution conformation and mutagenic specificity of 1, N^6-ethenoadenine. *IARC Sci. Publ.* 325–333.
(6) Fink, S. P., Reddy, G. R., and Marnett, L. J. (1997) Mutagenicity in Escherichia coli of the major DNA adduct derived from the endogenous mutagen malondialdehyde. *Proc. Natl. Acad. Sci. U.S.A. 94*, 8652–8657.
(7) Marnett, L. J., and Burcham, P. C. (1993) Endogenous DNA adducts: potential and paradox. *Chem. Res. Toxicol. 6*, 771–785.
(8) VanderVeen, L. A., Hashim, M. F., Nechev, L. V., Harris, T. M., Harris, C. M., and Marnett, L. J. (2001) Evaluation of the mutagenic potential of the principal DNA adduct of acrolein. *J. Biol. Chem. 276*, 9066–9070.
(9) Basu, A. K., Wood, M. L., Niedernhofer, L. J., Ramos, L. A., and Essigmann, J. M. (1993) Mutagenic and genotoxic effects of three vinyl chloride-induced DNA lesions: 1,N^6-ethenoadenine, 3,*N4*-ethenocytosine, and 4-amino-5-(imidazol-2-yl)imidazole. *Biochemistry 32*, 12793–12801.
(10) de los Santos, C., Kouchakdjian, M., Yarema, K., Basu, A., Essigmann, J., and Patel, D. J. (1991) NMR studies of the exocyclic 1, N^6-ethenodeoxyadenosine adduct (εdA) opposite deoxyguanosine in a DNA duplex. ε-dA(syn)·dG(anti) pairing at the lesion site. *Biochemistry 30*, 1828–1835.
(11) Swenberg, J. A., Boysen, G., Georgieva, N., Bird, M. G., and Lewis, R. J. (2007) Future directions in butadiene risk assessment and the role of cross-species internal dosimetry. *Chem.-Biol. Interact. 166*, 78–83.
(12) Morrow, N. L. (1990) The industrial production and use of 1,3-butadiene. *Environ. Health Perspect. 86*, 7–8.
(13) Hecht, S. S. (1999) Tobacco smoke carcinogens and lung cancer. *J. Natl. Cancer Inst. 91*, 1194–1210.
(14) Krause, R. J., and Elfarra, A. A. (1997) Oxidation of butadiene monoxide to meso- and (±)-diepoxybutane by cDNA-expressed human cytochrome P450s and by mouse, rat, and human liver microsomes: evidence for preferential hydration of meso-diepoxybutane in rat and human liver microsomes. *Arch. Biochem. Biophys. 337*, 176–184.

(15) Thornton-Manning, J. R., Dahl, A. R., Bechtold, W. E., Griffith, W. C., Jr., and Henderson, R. F. (1997) Comparison of the disposition of butadiene epoxides in Sprague-Dawley rats and B6C3F1 mice following a single and repeated exposures to 1,3-butadiene via inhalation. *Toxicology 123*, 125–134.
(16) Sasiadek, M., Norppa, H., and Sorsa, M. (1991) 1,3-Butadiene and its epoxides induce sister-chromatid exchanges in human lymphocytes in vitro. *Mutat. Res. 261*, 117–121.
(17) Cochrane, J. E., and Skopek, T. R. (1994) Mutagenicity of butadiene and its epoxide metabolites: I. Mutagenic potential of 1,2-epoxybutene, 1,2,3,4-diepoxybutane and 3,4-epoxy-1,2- butanediol in cultured human lymphoblasts. *Carcinogenesis 15*, 713–717.
(18) Henderson, R. F., Thornton-Manning, J. R., Bechtold, W. E., and Dahl, A. R. (1996) Metabolism of 1,3-butadiene: species differences. *Toxicology 113*, 17–22.
(19) Park, S., and Tretyakova, N. (2004) Structural characterization of the major DNA-DNA cross-link of 1,2,3,4-diepoxybutane. *Chem. Res. Toxicol. 17*, 129–136.
(20) Park, S., Hodge, J., Anderson, C., and Tretyakova, N. Y. (2004) Guanine-adenine cross-linking by 1,2,3,4-diepoxybutane: potential basis for biological activity. *Chem. Res. Toxicol. 17*, 1638–1651.
(21) Park, S., Anderson, C., Loeber, R., Seetharaman, M., Jones, R., and Tretyakova, N. (2005) Interstrand and intrastrand DNA-DNA cross-linking by 1,2,3,4-diepoxybutane: role of stereochemistry. *J. Am. Chem. Soc. 127*, 14355–14365.
(22) Verly, W. G., Brakier, L., and Feit, P. W. (1971) Inactivation of the T7 coliphage by the diepoxybutane stereoisomers. *Biochim. Biophys. Acta 228*, 400–406.
(23) Matagne, R. (1969) Induction of chromosomal aberrations and mutations with isomeric forms of L-threitol-1,4-bismethanesulfonate in plant materials. *Mutat. Res. 7*, 241–247.
(24) Kim, M. Y., Tretyakova, N. Y., and Wogan, G. N. (2007) Mutagenesis of the supF gene by stereoisomers of 1,2,3,4-diepoxybutane. *Chem. Res. Toxicol. 20*, 790–797.
(25) Zhang, X. Y., and Elfarra, A. A. (2003) Identification and characterization of a series of nucleoside adducts formed by the reaction of 2′-deoxyguanosine and 1,2,3,4-diepoxybutane under physiological conditions. *Chem. Res. Toxicol. 16*, 1606–1615.
(26) Zhang, X. Y., and Elfarra, A. A. (2004) Characterization of the reaction products of 2′-deoxyguanosine and 1,2,3,4-diepoxybutane after acid hydrolysis: formation of novel guanine and pyrimidine adducts. *Chem. Res. Toxicol. 17*, 521–528.
(27) Zhang, X. Y., and Elfarra, A. A. (2005) Reaction of 1,2,3,4-diepoxybutane with 2′-deoxyguanosine: initial products and their stabilities and decomposition patterns under physiological conditions. *Chem. Res. Toxicol. 18*, 1316–1323.
(28) Recio, L., Steen, A. M., Pluta, L. J., Meyer, K. G., and Saranko, C. J. (2001) Mutational spectrum of 1,3-butadiene and metabolites 1,2-epoxybutene and 1,2,3,4-diepoxybutane to assess mutagenic mechanisms. *Chem.-Biol. Interact. 135*−*136*, 325–341.
(29) Cochrane, J. E., and Skopek, T. R. (1994) Mutagenicity of butadiene and its epoxide metabolites: II. Mutational spectra of butadiene, 1,2-epoxybutene and diepoxybutane at the *hprt* locus in splenic T cells from exposed B6C3F1 mice. *Carcinogenesis 15*, 719–723.
(30) Antsypovich, S., Quirk Dorr, D., Pitts, C., and Tretyakova, N. (2007) Site specific N^6-(2-hydroxy-3,4-epoxybuty-1-yl)adenine oligodeoxynucleotide adducts of 1,2,3,4-diepoxybutane: synthesis and stability at physiological pH. *Chem. Res. Toxicol. 20*, 641–649.
(31) Quirk Dorr, D., Murphy, K., and Tretyakova, N. (2007) Synthesis of DNA oligodeoxynucleotides containing structurally defined N^6-(2-hydroxy-3-buten-1-yl)-adenine adducts of 3,4-epoxy-1-butene. *Chem.-Biol. Interact. 20*, 104–111.
(32) Ettlinger, M. G. (1950) Synthesis of the natural antithyroid factor l-5-vinyl-2-thioöxazolidone. *J. Am. Chem. Soc. 72*, 4792–4796.
(33) Kjaer, A., Christensen, B. W., and Hansen, S. E. (1959) Isothiocyanates. XXXIV. The absolute configuration of (−)-5-Vinyl-2-oxazolidinethione (goitrin) and its glucosidic progenitor (progoitrin). *Acta Chem. Scand. 13*, 144–150.
(34) Giese, T. J., Gregersen, B. A., Liu, Y., Nam, K., Mayaan, E., Moser, A., Range, K., Faza, O. N., Lopez, C. S., de Lera, A. R., Schaftenaar, G., Lopez, X., Lee, T.-S., Karypis, G., and York, D. M. (2006) QCRNA 1: A database of quantum calculations for RNA catalysis. *J. Mol. Graphics Modell. 25*, 423–433.
(35) Becke, A. D. (1988) Density-functional exchange-energy approximation with correct asymptotic behavior. *Phys. Rev. A: At., Mol., Opt. Phys. 38*, 3098–3100.
(36) Lee, C., Yang, W., and Parr, R. G. (1988) Development of the Colle-Salvetti correlation-energy formula into a functional of the electron density. *Phys. Rev. B: Condens. Matter 37*, 785–789.
(37) Wong, C. M., Buccini, J., and Te Raa, J. (1968) Synthesis of optically active deacetyl anisomycin. *Can. J. Chem. 46*, 3091–3094.
(38) Arakawa, Y., and Yoshifuji, S. (2007) Synthesis of (3S,4S)-3,4-dihydroxyprolines from L-tartaric acid. *Chem. Pharm. Bull. 39*, 2219–2224.
(39) Wan, Z. K., Binnun, E., Wilson, D. P., and Lee, J. (2005) A highly facile and efficient one-step synthesis of N^6-adenosine and N^6-2′-deoxyadenosine derivatives. *Org. Lett. 7*, 5877–5880.
(40) Goggin, M., Loeber, R., Park, S., Walker, V., Wickliffe, J., and Tretyakova, N. (2007) HPLC-ESI$^+$-MS/MS analysis of N7-guanine-N7-guanine DNA cross-links in tissues of mice exposed to 1,3-butadiene. *Chem. Res. Toxicol. 20*, 839–847.
(41) Singer, B. and Grunberger, D. (1983) *Molecular Biology of Mutagens and Carcinogens*, Plenum Press, New York and London.
(42) Maruenda, H., Chenna, A., Liem, L.-K., and Singer, B. (1998) Synthesis of *1,* N^6-ethano-2′-deoxyadenosine, a metabolic product of 1,3-bis(2-chloroethyl)nitrosourea, and its incorporation into oligomeric DNA. *J. Org. Chem. 63*, 4385–4389.
(43) Pawlowicz, A. J., Munter, T., Klika, K. D., and Kronberg, L. (2006) Reaction of acrolein with 2′-deoxyadenosine and 9-ethyladenine-formation of cyclic adducts. *Bioorg. Chem. 34*, 39–48.
(44) Singh, U. S., Decker-Samuelian, K., and Solomon, J. J. (1996) Reaction of epichlorohydrin with 2′-deoxynucleosides: characterization of adducts. *Chem.-Biol. Interact. 99*, 109–128.
(45) Fujii, T., and Itaya, T. (1999) Systematic tables of mono- and poly-N-methylated adenines: acid dissociation constants and UV and NMR spectral data. *Heterocycles 51*, 2255–2277.
(46) Macon, J. B., and Wolfenden, R. (1968) 1-Methyladenosine. Dimroth rearrangement and reversible reduction. *Biochemistry 7*, 3453–3458.
(47) Tretyakova, N., Sangaiah, R., Yen, T. Y., Gold, A., and Swenberg, J. A. (1997) Adenine adducts with diepoxybutane: isolation and analysis in exposed calf thymus DNA. *Chem. Res. Toxicol. 10*, 1171–1179.
(48) Mikhailov, S. N., Rozenski, J., Efimtseva, E. V., Busson, R., Van Aerschot, A., and Herdewijn, P. (2002) Chemical incorporation of 1-methyladenosine into oligonucleotides. *Nucleic Acids Res. 30*, 1124–1131.
(49) Byrns, M. C., Vu, C., and Peterson, L. A. (2004) The formation of substituted 1,N^6-etheno-2′-deoxyadenosine and 1,N^2-etheno-2′-deoxyguanosine adducts by cis-2-butene-1,4-dial, a reactive metabolite of furan. *Chem. Res. Toxicol. 17*, 1607–1613.
(50) Selzer, R. R., and Elfarra, A. A. (1996) Characterization of N1- and N6-adenosine adducts and *N*1-inosine adducts formed by the reaction of butadiene monoxide with adenosine: evidence for the N1-adenosine adducts as major initial products. *Chem. Res. Toxicol. 9*, 875–881.
(51) Chang, C. J., Ashworth, D. J., Chern, L. J., Gomes, J. D., Lee, C. G., and Narayan, R. (1984) ^{13}C NMR studies of methylnucleosides. *Org. Magn. Reson. 12*, 671–675.
(52) Jayaraj, K., Georgieva, N. I., Gold, A., Sangaiah, R., Koc, H., Klapper, D. G., Ball, L. M., Reddy, A. P., and Swenberg, J. A. (2003) Synthesis and characterization of peptides containing a cyclic Val adduct of diepoxybutane, a possible biomarker of human exposure to butadiene. *Chem. Res. Toxicol. 16*, 637–643.
(53) Smith, R. A., Williamson, D. S., Cerny, R. L., and Cohen, S. M. (1990) Detection of 1, N^6- propanodeoxyadenosine in acrolein-modified polydeoxyadenylic acid and DNA by ^{32}P postlabeling. *Cancer Res. 50*, 3005–3012.
(54) Shallop, A. J., Gaffney, B. L., and Jones, R. A. (2003) Use of 13C as an indirect tag in ^{15}N specifically labeled nucleosides. Syntheses of [8-^{13}C-1,7, NH_2-$^{15}N_3$]adenosine, -guanosine, and their deoxy analogues. *J. Org. Chem. 68*, 8657–8661.
(55) Sugiyama, T., Schweinberger, E., Kazimierczuk, Z., Ramzaeva, N., Rosemeyer, H., and Seela, F. (2000) 2-aza-2′-deoxyadenosine: synthesis, base-pairing selectivity, and stacking properties of oligonucleotides. *Chemistry 6*, 369–378.
(56) Kemper, R. A., Krause, R. J., and Elfarra, A. A. (2001) Metabolism of butadiene monoxide by freshly isolated hepatocytes from mice and rats: different partitioning between oxidative, hydrolytic, and conjugation pathways. *Drug Metab. Dispos. 29*, 830–836.
(57) Silva, L. C., Alvarez, R., Dominguez, M., Nieto, F. O., and de Lera, A. R. (2009) Complex thermal behavior of 11-*cis*-retinal, the ligand of the visual pigments. *J. Org. Chem. 74*, 1007–1013.
(58) Scholdberg, T. A., Nechev, L. V., Merritt, W. K., Harris, T. M., Harris, C. M., Lloyd, R. S., and Stone, M. P. (2005) Mispairing of a site specific major groove (2S,3S)-*N*6-(2,3,4-trihydroxybutyl)-2′-deoxyadenosyl DNA adduct of butadiene diol epoxide with deoxyguanosine: formation of a dA(anti)·dG(anti) pairing interaction. *Chem. Res. Toxicol. 18*, 145–153.

TX900312E